Journal of Molecular Structure 1289 (2023) 135775

Contents lists available at ScienceDirect

Journal of Molecular Structure

journal homepage: www.elsevier.com/locate/molstr

Synthesis, antimicrobial activity, electrochemical studies and molecular modeling studies of novel 1,3,4-oxadiazole derivatives

Amal A. AL-Sharabi [a,*], Sana Saffour [a], Asaf Evrim Evren [a,b], Gizem Bayazıt [c], Gülşah Çongur [b], Ülküye Dudu Gül [d], Leyla Yurttaş [a]

[a] Anadolu University, Faculty of Pharmacy, Department of Pharmaceutical Chemistry, 26470, Eskişehir, Turkey
[b] Bilecik Seyh Edebali University, Vocational School of Health Services, Department of Pharmacy Services, Bilecik 11000, Turkey
[c] Bilecik Seyh Edebali University, Department of Biotechnology, Institute of Graduate Studies, Bilecik, Turkey
[d] Bilecik Seyh Edebali University, Faculty of Engineering, Department of Bioengineering, Bilecik 11230, Turkey

ARTICLE INFO

Keywords:
1,3,4- Oxadiazole
Antibacterial activity
Antifungal activity
Electrochemical measurements
Molecular docking
Molecular dynamic simulation

ABSTRACT

The high incidence of antimicrobial-resistant (AMR) infections in recent decades has made the development of novel antimicrobial medications one of the medicinal chemists' top priorities. In this study, synthesis, *in vitro* antimicrobial activity, electrochemical studies, *in silico* pharmacokinetic ADME parameters, molecular docking, and molecular dynamic simulations were all performed on several 1,3,4-oxadiazole derivatives. The minimum inhibitory concentrations (MIC) of these compounds were evaluated against eleven species of gram-positive bacteria, gram-negative bacteria and fungal pathogens using azithromycin as the reference antibacterial agent, voriconazole and fluconazole as the reference antifungal agents. Both compounds **4d** and **4f** were found to be approximately as effective as azithromycin against *E. faecalis* and *E. coli*, respectively while three compounds showed antifungal activity against *C. parapsilopsis*, with MIC values that were identical to fluconazole for **4g** and **4i**, and to voriconazole for **4j**. Also, the most potent derivatives-double stranded DNA (dsDNA) interactions were evaluated using an electrochemical technique. Compounds **4d, 4f** and **4i** were found to disrupt the structure of dsDNA however compound **4h** wasn't able to bind to dsDNA. In addition, the structure-activity relationship (SAR) of compounds **4f** and **4d** were elucidated by molecular modeling studies.

1. Introduction

Both overprescription and misuse of antimicrobial drugs have been linked to the acceleration of microbial genetic changes that result in increased microbial resistance to clinically available antimicrobial drugs. This dramatic rise in antimicrobial resistance (AMR) has significantly raised the cost burden on governments, as well as morbidity and mortality, particularly among immunocompromised patients and those with chronic conditions [1], making AMR one of the top ten global public health crises threatening humanity, according to the World Health Organization (WHO) [2]. Hence, the negative consequences of AMR have highlighted the urgent need for novel antimicrobial compounds with improved or at least comparable efficacy and safety profiles.

Heterocyclic rings are now a major focus of research in medicinal chemistry. Remarkably, many designed antimicrobial novel compounds involve at least one heterocycle ring [3]. One of these is oxadiazole, a five-membered heterocyclic ring that contains two carbon atoms, two nitrogen atoms, and one oxygen atom. Most studies that investigated oxadiazole in the literature were primarily concerned with the 1,3,4-oxadiazole isomer compared to the other less investigated isomers which are 1,2,3-oxadiazole, 1,2,4-oxadiazole, and 1,2,5-oxadiazole, and this is due to the enormously wide range of therapeutical activities of 1,3,4-oxadiazole including antimicrobial [4–10], anti-tubercular, anti--viral, anthelmintic, antiprotozoal, antioxidant, anti-inflammatory, analgesic, anti-allergic, anticonvulsant, antitumor, hypoglycemic, anti-Alzheimer, and antihypertensive activities [11,12]. Besides that, there are FDA-approved clinical drugs on the market that contain the 1,3,4-oxadiazole moiety (Fig. 1) such as furamizole, raltegravir, nesapidil, zibotentan, and tiodazosin, which are used as antibacterial, antiviral, anti-arrhythmic, anticancer, and antihypertensive agents, respectively [13,14].

As introducing another active heterocyclic ring can broaden the spectrum of antimicrobial activity, thiazole and benzothiazole moiety

* Corresponding author.
E-mail address: amal_anfa@anadolu.edu.tr (A.A. AL-Sharabi).

https://doi.org/10.1016/j.molstruc.2023.135775
Received 23 December 2022; Received in revised form 18 April 2023; Accepted 12 May 2023
Available online 18 May 2023

were also introduced to the main 1,3,4-oxadiazole nucleus. Structurally, thiazole and benzothiazole contain nitrogen and sulfur atoms as part of a five-membered ring; however, the five-membered ring in benzothiazole is further attached to a benzene ring at the fourth and fifth carbons. Both thiazole and benzothiazole are well-known for their immense biological activities [15–21], however, antimicrobial activity is attributed largely to these activities [22–25]. Thiazole is a cornerstone of many antimicrobial natural products and clinically approved drugs, such as bacitracin, different penicillins, ceftriaxone, sulfathiazole, ritonavir, abafungin, tiabendazole, abafungin, ritonavir, ruvaconazole and azereonam. Additionally, many drugs contain benzothiazole derivatives in their structures, including riluzole [26] (neuroprotective drug), dimazole (antifungal), ethoxolamide (diuretic) and pramipexole (anti-parkinson drug) [27].

Drugs having heterocyclic rings have been widely investigated to enlight their effects on DNA structure [28–31]. Their heterocyclic groups can place between the complementary DNA bases resulting in intercalation [32,33], or these drugs can act as groove binders [33]. Moreover, there were several reports that oxadiazole ring interaction with dsDNA [34–36]· Based on 1,3,4-oxadiazole's affinity on dsDNA, as DNA gyrase and thymidylate synthase enzymes have role in producing DNA, several enzymatic studies declared that these two enzymes are inhibited in these organisms by also oxadiazole nuclei [37–43]. Several analytical techniques can be applied to investigate drug-DNA interactions [33], but electrochemical techniques are more prominent since they are suitable for the development of biosensors to monitor drug-DNA interactions. Accurate and sensitive results for the evaluation of the interaction between selected drug and DNA are obtained using the electrochemical biosensors without the necessity of exhausting and time-consuming experimental procedures. As a result of this advantage, state-of-art reports widely include the investigation of the mechanisms of new drugs on DNA structure using the principles of electrochemical biosensor technologies [33,44–47].

According to Salama's study in 2020, derivatives containing 1,3,4-oxadiazole core, substituted benzyl in the 5th position and benzoyl amino/phenylacylamino/benzothiazol-2-ylmercaptoacylamino in the 2nd position were synthesized and exhibited strong activity against *Salmonella typhi* [48]. On the other hand, Akhtar et al. designed similar compounds by focusing on the reported antitumoral activities of 1,3,4-oxadiazole and 2-aminobenzothiazole rings. These compounds were determined to exhibit potent activity on leukemia cells and were also tested on RNA to define antiviral capacity [49]. Based on the aforementioned studies and the wide biodiversity of the ring systems, especially the antimicrobial and anticancer, we created a model with a linker between the benzothiazole/thiazole rings in the 2nd position on the 1,3,4-oxadiazole core and phenoxymethyl residues in the 5th position (Fig. 2). On this model, we performed biological tests by providing substituent changes on the benzothiazole and thiazole rings. The synthesized 2,5-disubstituted-1,3,4-oxadiazole derivatives were characterized by IR, ^{1}H NMR, ^{13}C NMR and HR-MS and tested for their *in vitro* antibacterial and antifungal activities. Also, molecular docking studies and molecular dynamic simulation studies were performed for the most active compounds in addition to the determination of the *in silico* ADME parameters. Moreover, the interaction between the derivatives and dsDNA was studied using a disposable electrochemical biosensor platform to evaluate how the derivatives affected the dsDNA structure.

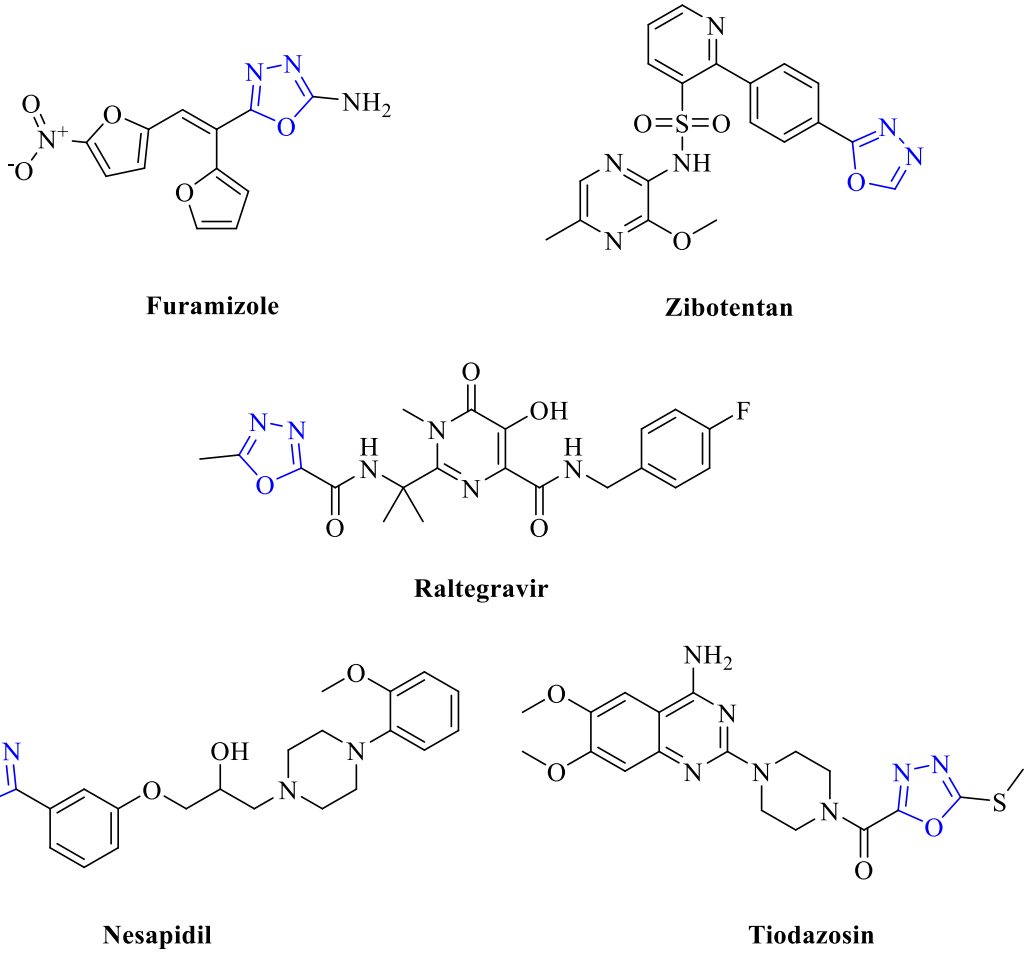

Fig. 1. 1,3,4-Oxadiazole containing approved drugs.

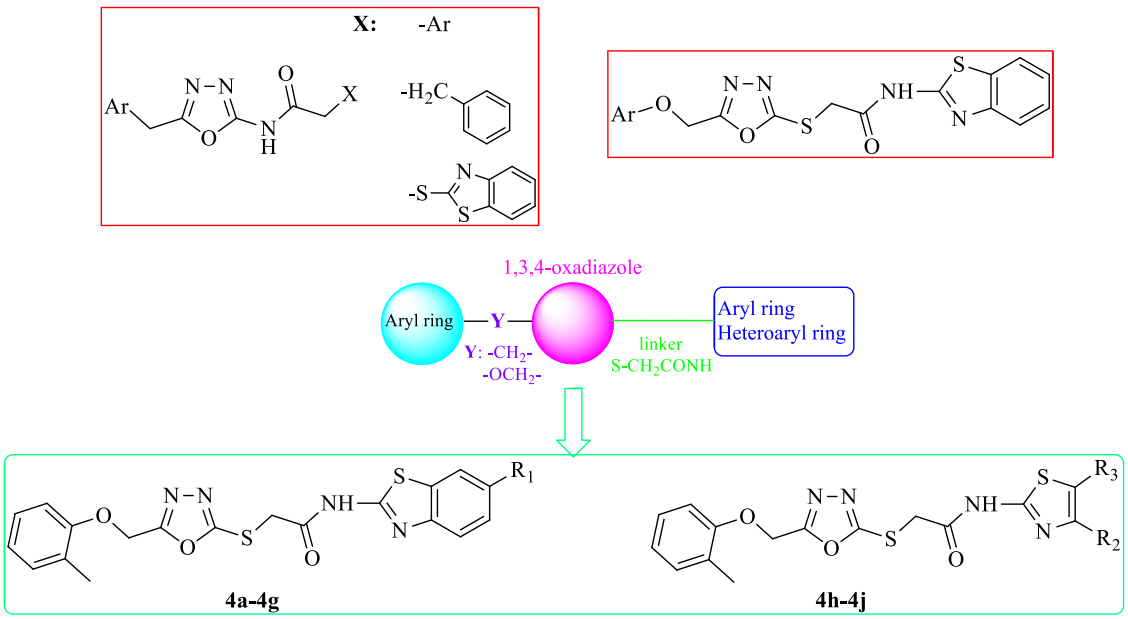

Fig. 2. Designing protocol of the compounds.

Consistency of the results obtained by different techniques were evaluated.

2. Results and discussion

2.1. Chemistry

A total of ten compounds were synthesized using *o*-cresol (2-methyl phenol) as the first starting material which was refluxed for 5 h with ethyl bromoacetate in acetone and K_2CO_3 to produce ethyl 2-(o-tolyloxy)acetate **(1)** that was further refluxed for 7 h with hydrazine monohydrate in ethanol to produce 2-(o-tolyloxy)acetohydrazide **(2)**. Afterwards, compound **(2)** was cyclized into 5-((o-tolyloxy)methyl)–1,3,4-oxadiazole-2-thiol **(3)** using CS_2 in 2 N NaOH/EtOH solution. In the final step, compound **(3)** was substituted at position 2 with different benzothiazole or thiazole substituents to give compounds **4a-4g** and **4h-4j**, respectively as illustrated in Scheme 1. Final compounds were obtained in a good yield of 70–80%. IR, ^{1}H NMR, ^{13}C NMR and HRMS were used to evaluate purity and establish the chemical structures of the compounds (**Figs. S1-S40**, Supplementary data).

In the IR spectra of the compounds, characteristic N—H, C=O and C—O bonds were observed at 3200–3172 cm^{-1}, 1699–1666 cm^{-1} and 1269–1005 cm^{-1}, respectively. Additionally, other bands belong to C=C, C—H and benzene ring out-of-plane deformation bands were also observed at expected regions.

In the ^{1}H NMR spectra of the compounds, all the aliphatic protons of

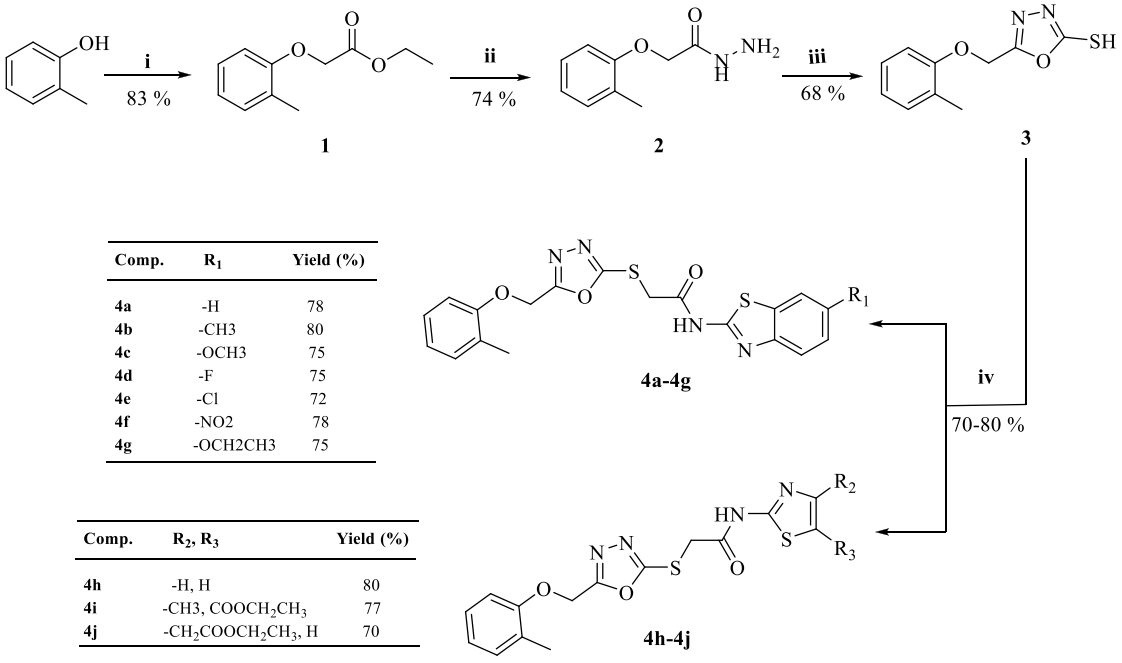

Comp.	R_1	Yield (%)
4a	-H	78
4b	-CH3	80
4c	-OCH3	75
4d	-F	75
4e	-Cl	72
4f	-NO2	78
4g	-OCH2CH3	75

Comp.	R_2, R_3	Yield (%)
4h	-H, H	80
4i	-CH3, $COOCH_2CH_3$	77
4j	$-CH_2COOCH_2CH_3$, H	70

Scheme 1. *Synthesis of compounds **(4a-4j)***. **i**: ethyl bromoacetate, acetone/K_2CO_3, reflux, 5 h; **ii**: $NH_2NH_2.H_2O$, EtOH, reflux, 7 h; **iii**: CS_2, 2 N NaOH/EtOH, reflux, 5 h; **iv**: 2-chloro-*N*-(benz/thiazol-2-yl)acetamides, acetone/K_2CO_3, R.T.

Ph—CH_3 were found to have a signal at about 2.11–2.13 ppm while other aliphatic S-CH_2 and O—CH_2 protons were found to resonate at about 4.33–4.47 and 5.37–5.39 ppm, respectively. For aromatic protons, the four protons of phenyl, the protons of thiazole and the protons of benzothiazole were found to resonate as expected at about 6.89–9.0 ppm. Amide proton was found to resonate at about 12.54–12.98 ppm in almost all compounds.

In the ^{13}C NMR spectra of the compounds, aliphatic carbon signals were detected upfilded to the right of the spectrum with the common aliphatic carbons Ph—CH_3, S-CH_2, and O—CH_2 at about 16.28–18.4,

35.87–37.41 and 60.16–60.19 ppm, respectively. Downfilded the spectra, aromatic carbons signals range at about 112.68–164.82 ppm, except for **4c, 4d** and **4g** containing OCH_3, F and OCH_2CH_3, respectively at the sixth position of benzothiazole which had signals ranging from 105.15 to 164.71 ppm, also for **4j** containing ethoxy carbonyl methyl at the fourth position of thiazole which was found to has a signal at 110–165.9 ppm. Additionally, the signal of carbonyl amide carbon was found to be at the most deshielded shift at about 163.67–170.51 ppm.

According to the $[M+H]^+$ HR-MS results, the compounds' molecular weights were perfectly consistent with the theoretical calculations, with the difference beginning in the third decimal point which shows the compounds have acceptable purity.

2.2. Antimicrobial activity

The antimicrobial activity of compounds **4a-4j** was determined by finding MIC values as shown in Tables 1 and 2.

Antibacterial activity of all synthesized compounds was evaluated against four Gram-positive and four Gram-negative bacterial pathogens; *E. coli, S. marcescens, K. pneumoniae, P. aeruginosa, E. faecalis, B. subtilis, S. aureus and S. epidermidis*. Whereas antifungal activity was tested against three fungal microorganisms: *C. albicans, C. krusei and C. parapsilopsis*. Azithromycin was used as a standard antibacterial agent, whereas voriconazole and fluconazole were used as standard antifungal agents.

The antibacterial activity results demonstrated that compound **4d** exhibited a considerable antibacterial activity against *E. faecalis* (MIC 0.97 μg/mL). While compound **4f** showed remarkable activity against *E. coli* at the same potency (MIC 0.97 μg/mL) which is almost identical to the activity of the reference agent azithromycin. However, **4h** was inactive (MIC> 250 μg/mL) against *E. coli*. The MIC of compounds **4b, 4c, 4d, 4e, 4i** and **4j** against *E. coli* was found to be 31.25 μg/mL, while it needed two folds of that concentration from **4a** (MIC 62.5 μg/mL) to achieve the same activity. For compounds **4a, 4b, 4c, 4e** and **4f**, the MIC against *E. faecalis* was found to be 15.625 μg/mL, while it required only half of that concentration from **4j** (7.81 μg/mL) to inhibit the same strain of bacterial pathogen. All compounds were inactive against *S. marcescens, K. pneumoniae, P. aeruginosa, B. subtilis, S. aureus, and S. epidermidis.*

According to the antifungal activity results, **4g** and **4i** (MIC 3.90 μg/mL) displayed a noticeable antifungal activity against *C. parapsilopsis* at the same concentration as fluconazole (MIC 3.90 μg/mL). Whereas **4j** (MIC 1.95 μg/mL) showed the same inhibitory effect of voriconazole against *C. parapsilopsis*. This outcome confirms that ethoxy in benzothiazole (**4g**) and ethoxy carbonyl in thiazole (**4i** and **4j**) are supposed to have a considerable influence on antifungal activity against the tested *C. parapsilopsis* pathogen. For compound **4h**, (MIC 15.625 μg/mL) demonstrated inhibitory action at the quarter potency of fluconazole (MIC 3.90 μg/mL) against *C. parapsilopsis*. While it was found that it needed 8-fold more concentration from **4b, 4c, 4d, 4e**, and **4f** (MIC 31.25 μg/mL) to inhibit *C. parapsilopsis* growth compared to fluconazole (MIC 3.90 μg/mL). It was also revealed that most of the tested compounds possessed a good activity against *C. albicans*. Compounds **4a, 4b, 4f** and **4 g** (MIC 15.625 μg/mL) showed good anticandidal activity against *C. albicans* at half potency of fluconazole (MIC 7.81 μg/mL). While **4e** (MIC 31.25 μg/ml) demonstrated inhibitory action at the quarter potency of fluconazole (MIC 7.81 μg/mL) against *C. albicans*. **4c** and **4i** (MIC 62.5 μg/mL) required an 8-fold increase in concentration to reveal fluconazole's inhibitory effect (MIC 7.81 μg/mL) against *C. albicans*.

When the antimicrobial effects and structures of the compounds are examined, there is no clear difference between those containing benzothiazole and thiazole, but it varies according to the substituents these two groups carry. Significant antibacterial activity was observed against *E. coli* and *E. faecalis* in molecules containing F **(4d)**, NO_2 **(4f)** and OC_2H_5 **(4 g)** substituents in benzothiazole containing derivatives. Derivatives containing thiazole **(4h)**, and thiazole with CH_3 at 4th position and COOEt at 5th position **(4i)** were detected for their remarkable antibacterial activity. The efficiency against fungi was higher than the efficiency against bacteria, implying that the produced compounds have higher antifungal than antibacterial activity. It is anticipated that antifungal activity may be influenced by the presence of ethoxy/ ethoxy carbonyl linked to benzothiazole/ thiazole rings. It was determined that compounds **4g, 4i** and **4j**, which carry the highest number of carbon-

Table 2
Antifungal activity of the compounds **4a-4j**. (*: most active compounds).

Compound no.	Minimum inhibitory concentration (MIC) in μg/mL		
	C. albicans	*C. krusei*	*C. parapsilopsis*
4a	15.625*	125	62.5
4b	15.625*	125	31.25
4c	62.5	125	31.25
4d	125	125	31.25
4e	31.25	62.5	31.25
4f	15.625*	62.5	31.25
4g	15.625*	125	3.90*
4h	31.25	125	15.625
4i	62.5	62.5	3.90*
4j	125	62.5	1.95*
Voriconazole	3.90	3.90	1.95
Fluconazole	7.81	7.81	3.90

Table 1
Antibacterial activity of the compounds **4a-4j**. (*: most active compounds).

	Minimum inhibitory concentration (MIC) in μg/mL							
	Gram-negative bacteria				Gram-positive bacteria			
	E. coli	*S.marcescens*	*K.pneumoniae*	*P.aeruginosa*	*E.faecalis*	*B.subtilis*	*S.aureus*	*S.epidermidis*
4a	62.5	125	125	125	15.625	125	125	62.5
4b	31.25	62.5	125	125	15.625	125	125	31.25
4c	31.25	125	125	62.5	15.625	125	62.5	62.5
4d	31.25	125	125	125	0.97*	125	125	125
4e	31.25	62.5	125	125	15.625	125	125	125
4f	0.97*	125	125	125	15.625	125	125	125
4g	1.9*	125	125	125	3.90*	250	125	125
4h	> 250	125	125	125	1.95*	250	125	125
4i	31.25	62.5	125	125	1.95*	125	125	125
4j	31.25	62.5	125	125	7.81	125	125	125
Azithromycin	< 0.97	< 0.97	< 0.97	< 0.97	< 0.97	< 0.97	< 0.97	< 0.97

containing substituents, attracted attention with high MIC values of antifungal activity.

2.3. Electrochemical studies

The electrochemical interaction between dsDNA and the derivatives was investigated in this part of our study. First, the electrochemical behavior of the compounds was studied to monitor whether there would be overlapping with the guanine oxidation signal and the compounds (**Fig. S41**–Supplementary data). For this purpose, the compounds at their MIC level were immobilized at the surface of the PGEs, then, voltammetric measurements were performed. The guanine oxidation signal was observed at +1.025 V while the oxidation signals of derivatives **4d, 4h** or **4i** were measured at +0.950 V, +1.00 V and +1.075 V as 103 nA, 1050 nA and 573 nA, respectively. On the other hand, the oxidation signal of compound **4d** was smaller than derivatives **4f** or **4i**, and it was considered that the signal of derivative **4d** is negligible. However, the other signals could overlap with the guanine signal and negatively affect the ability to make correct decisions about the interaction process. Therefore, derivative **4d** was chosen as the model derivative and further experiments were performed with this compound.

The effect of interaction time on the interaction process done between 0.95 μg/mL of derivative **4d** and 30 μg/mL of dsDNA was investigated by performing the interaction for different interaction times from 5 to 60 mins. The voltammograms of the guanine signals of derivative **4d** signals were represented in **Fig. S42**-Supplementary data and the average guanine signals were given in Fig. 3. In principle, the guanine oxidation signal is measured before/after each interaction step and the changes at the guanine signal are evaluated in terms of the interaction process when an voltammetric biosensor system is aimed to use for the evaluation of drug DNA interactions. The average guanine signal was measured as 5.50 ± 0.56 μA with the relative standard deviation% (RSD%)= 10.20% ($n = 3$) (Fig. 3-a). The signal of derivative **4d** was noticed to be decreased while the interaction time increased (Fig. 3-b). There were 5.05% increase while 19.92%, 16.16% and 7.00% decreases at the guanine signal after the interaction of dsDNA and derivative **4d** during 5, 15, 30, and 60 min, respectively (Fig. 3-c). The decrease at the guanine signal was obtained after the interaction process due to the formation of strand breaks at the dsDNA as a result of the binding of derivative **4d** due to its planar structure. This result was in parallel with the other reports that covered the voltammetric monitoring of novel iron (III) and nickel (II) complexes and DNA interaction [50], topotecan and DNA interaction [51], and daunorubicin-DNA interaction [52].

The most significant decrease at the guanine signal was obtained after 15 min interaction (**Fig. S42-B**, c to D- Supplementary data) and the average guanine signal was measured as 4.41 ± 0.29 μA (RSD%= 6.57%, $n = 3$) (Fig. 3, 15 min-c). Further experiments were performed using 15 min interaction time.

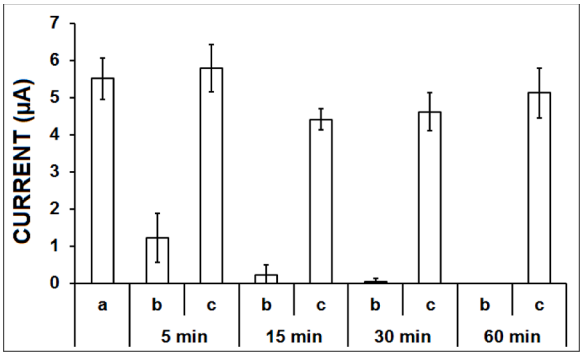

Fig. 3. The average guanine signal obtained using 30 μg/mL dsDNA modified PGE (a), the control signals of **4d** after the immobilization of 0.95 μg/mL **4d** at the surface of the PGEs for 5–60 min (b), the average guanine signals (c) obtained after the interaction of 30 μg/mL dsDNA and of 0.95 μg/mL derivative **4d** for 5–60 min at the surface of the PGEs (n=3).

The interaction between the derivatives and the dsDNA was investigated using the EIS technique which is a powerful and reliable electrochemical method widely used to understand and evaluate step-by-step modification/interaction processes performed at the electrode surface. Briefly, the real (Z') and imaginary (-Z'') components comprise of the complex impedance. R_{ct} is defined as the charge transfer resistance which indicates the resistance value occurred at the electrode/electrolyte interface, and this value is represented as the semicircle diameter of the Nyquist diagram. The impedance data are fitted using an equivalent circuit model (herein Randles model represented as inset in Fig. 4A-D). The other elements of the equivalent circuit model are the solution resistance (R_s), the capacitance (Q), and Warburg impedance (W) [50–52].

The average R_{ct} values ($n = 3$) obtained after each modification/interaction step and the Nyquist diagrams were represented in Fig. 4. The average R_{ct} value was found to be 79.67 Ohm (RSD%=19.22%, n=3) using the PGEs (Fig. 4E). After the modification of dsDNA at the surface of the PGE, the R_{ct} value sharply increased (Fig. 4E) and the average R_{ct} value was found to be 957.83 ± 108.66 Ohm (RSD%= 11.34%, $n = 3$). The negatively charged dsDNA caused to increase in the repulsive interaction between the electrode/electrolyte interface and resulted in obtaining an increment after the dsDNA modification. The average R_{ct} value increased after the interactions of dsDNA and derivatives **4d** (Fig. 4E), **4f** (Fig. 4E) or **4i** (Fig. 4E) whereas almost no change could be obtained at the average R_{ct} value after the interaction of compound **4h** and dsDNA (Fig. 4E). The increased ratios at the average R_{ct} value were calculated as 31.54%, 85.47% and 32.94% and the average R_{ct} values were measured as 1260.00 ± 14.14 Ohm (RSD%= 1.12%, $n = 3$), 1776.50 ± 201.53 Ohm (RSD%=11.34%, $n = 3$), and 1273.33 ± 148.79 Ohm (RSD%= 11.68%, $n = 3$) after the interaction between dsDNA and compounds **4d, 4f** or **4i**, respectively. The derivatives were also studied without the interaction process to check the electrochemical behavior of them. As it can be seen in Fig. 4, all compounds caused to increase at the R_{ct} value (Fig. 4A-D, from a to b). After the interaction of dsDNA and compounds **4d, 4f** or **4i**, negatively charged derivatives bound the dsDNA structure and caused the formation of strand breaks. Therefore, the average R_{ct} values increased. On the other hand, it is possible to conclude that compound **4h** could not bind to dsDNA as almost there was no increase at the average R_{ct} value and a reproducible average R_{ct} value could not be obtained.

2.4. ADME parameters

Molsoft software [53] and the SwissADME [54] programs were used to compute the ADME properties of the target compounds **4a-4j** as shown in Table 3. The molecular weights ranged from 362.43 to 457.48. Partition coefficient values between octanol and water (log P) varied between 2.46 and 4.1. Water solubility (Log S) and skin permeation (Log Kp) logarithms were estimated in the ranges of 3.77 to 5.32 and −5.63 to −6.96, respectively. The DLMS (drug-likeness model score) ranged between −0.47 to 0.50. For all synthesized compounds, the number of hydrogen bond donors (HBD) was 1, whereas the number of hydrogen bond acceptors (HBA) was between 6 and 8. Molecular volumes and Topological polar surface areas (TPSA) were determined between 312.79 to 424.95 $Å^3$ and 143.68 to 189.5 $Å^2$, respectively. According to Lipinski's rule, none of the synthesized compounds deviated from the rule which means that they may be orally available agents after prerequisite modifications in the future.

2.5. Molecular docking

Docking studies were first performed to assess the binding interactions of the most active compounds **4d, 4f, 4i** and **4h** within dsDNA

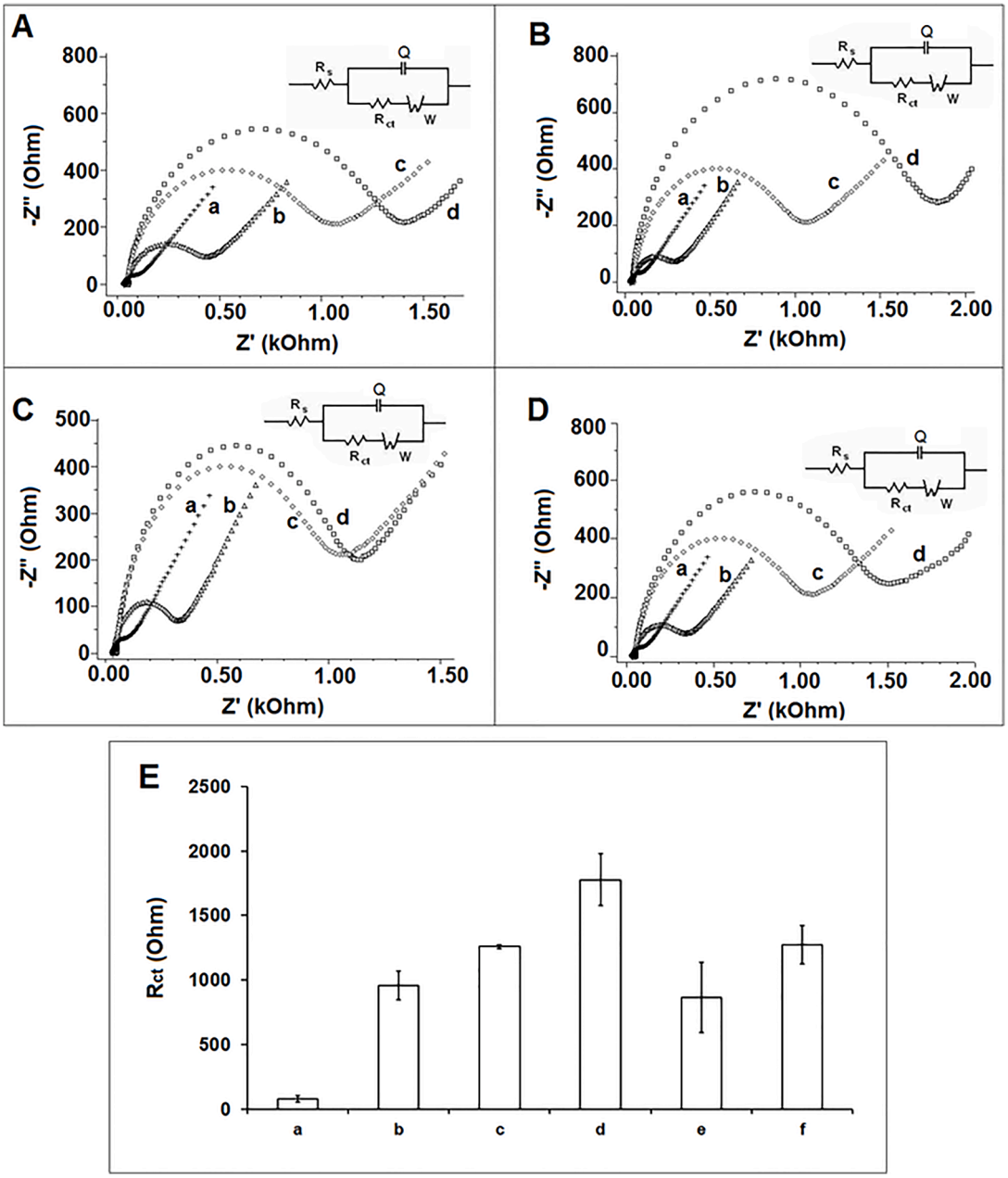

Fig. 4. The Nyquist diagrams obtained before and after the interaction of 30 μg/mL dsDNA and 0.97 μg/mL of **4d** (A) or **4f** (B) and 1.95 μg/mL of **4h** (C) or **4i** (D) at the surface of the PGEs during 15 min. PGE (a), controls of **4d, 4f, 4h** and **4i** (b), dsDNA modified PGE (c), the interaction between dsDNA and **4d, 4f, 4 h** or **4i** (d). Inset: The Randles circuit applied to fit the impedance data. Charge transfer resistance value (R_{ct}): The respective semicircle diameter regarding the charge-transfer resistance occurred between the PGE and the electrolyte, R_s: The solution resistance, Q: The capacitance, and W: Warburg impedance. The average R_{ct} values (E) obtained by PGEs (a), 30 μg/mL dsDNA modified PGEs (b), after the interaction between 30 μg/mL dsDNA and 0.95 μg/mL of **4d** (c) or **4f** (d) and 1.95 μg/mL of **4h** (e) or **4i** (f) ($n = 3$).

to further explain the results of the EIS technique (Fig. 5-A). Compound **4d** which was found to have both the most activity against *E. faecalis* and the most decrease in the guanine signal showed to have four binding interactions (Figs. 5-B1 and B2). The first is a π-π stacking interaction of the phenyl moiety within the heterocyclic benzothiazole system with the pyrimidine moiety of A:DG4 nucleotide. The other three are aromatic hydrogen bond interactions (Ar H-bond), two of them are between the hydrogens of the methyl group in the compound and the carbonyl groups of two thymine nucleotides DT7 and DT19 and the third is between the H_5 of benzothiazole moiety and the carbonyl group of DC23. For compound **4f** which showed the most activity against *E.coli*, two hydrogen bond interactions were noticed (Fig. 5-C1). The first is between the oxygen of the ether group and B:DG22 while the second is between the -NH of the amidic group and A:DA6. The H_4 and H_5 of the benzothiazole moiety were found to form additional two Ar H-bond interactions with DT19 and DT7, respectively (Fig. 5-C2). Compound **4i** which has significant activity against *E.faecalis* was found to bind B:DG22 by two hydrogen bond interactions with its -NH of the amidic group and C=O of the ester group (Fig. 5-D1). The H_4 and H_5 of the phenyl moiety were found to participate in additional two Ar H-bond interactions with DT7 and DT19, respectively (Fig. 5-D2). Compound **4h** was found to have significant *in vitro* activity against *E. faecalis*, however the results of the EIS technique showed that compound **4h** can not bind to dsDNA as the average R_{ct} value did not increase. The result of the docking study of compound **4h** is in harmony with the EIS results as only one Ar H-bond interaction is noticed between H_3 of the phenyl group

Table 3
Calculated values of the ADME parameters.

Molecule	MW	HBA	HBD	TPSA	Log P	Log S	Log Kp	MV	DLMS	NoV
4a	412.49	6	1	143.68	3.61	−5.01	−5.87	374.48	0.35	0
4b	426.51	6	1	143.68	3.84	−5.31	−5.69	395.50	0.02	0
4c	442.51	7	1	152.91	3.6	−5.08	−6.07	406.40	0.21	0
4d	430.48	7	1	143.68	3.89	−5.17	−5.91	380.47	0.31	0
4e	446.93	6	1	143.68	4.1	−5.6	−5.63	–	–	0
4f	457.48	8	1	189.5	2.97	−5.07	−6.26	399.54	−0.47	0
4g	456.54	7	1	152.91	3.89	−5.32	−5.9	424.96	0.19	0
4h	362.43	6	1	143.68	2.46	−3.77	−6.57	321.79	0.50	0
4i	448.52	8	1	169.98	3.26	−4.61	−6.42	416.09	0.43	0
4j	448.52	8	1	169.98	2.82	−4.06	−6.96	413.11	0.33	0

MW: Molecular weight, HBA: Number of hydrogen acceptors, HBD: Number of hydrogen donors, TPSA: Topological polar surface area ($Å^2$) Log P: Octanol/water partition coefficient, Log S: Aqueous solubility (the decimal logarithm of the molar solubility in water), Log Kp: Skin permeation constant (cm/s), MV: Molecular volume ($Å^3$), DLMS: Drug-likeness model score, NoV: Number of Violation (Lipinski's). DLMS and MV were calculated by molsoft.com/mprop. MW, Log P, Log S, Log Kp, TPSA, HBA, HBD and NoV were calculated by http://www.swissadme.ch/index.php.

and DC21 (Fig. 5-E). Compound **4h** may not show its antimicrobial activity as DNA poison and moreover, its activity may be based on only the inhibition of enzymatic reactions of the microbial organism. For instance, alanine racemase and D-alanine–D-alanine ligase inhibitors targets cell wall peptidoglycan synthetic pathway. Other compounds work on vital bacterial components including bacterial ribosome, sortase enzyme, lipid II and lipid III. Bacterial growth might also be inhibited by interfering with teichoic acid biosynthesis [55].

The docking results of the binding interactions of the most active compound against *E. coli* **4f** with DNA gyrase as the drug target were represented as 2D and 3D in Fig. 6-A and Fig. 6-B, respectively. The phenyl group of the compound was found to participate in two π-π stacking interactions with H:DA2011 and G:DA2011. The oxygen of the nitro group binds to B:ARG1122 by hydrogen bond interaction while the H_7 of the benzothiazole moiety binds to ASP1083 by Ar H-bond interaction.

On the other hand, the docking studies of the binding interactions of the most active compound against *E.faecalis* **4d** within TS as another possible drug target were represented as 2D and 3D in Fig. 6-C and D, respectively. The thiazole ring of benzothiazole moiety bind to PHE227 by a π-π stacking interaction while the N_3 of the oxadiazole ring binds to TYR145 by hydrogen bond interaction. Both H_3 and H_4 of the phenyl group form two Ar H-bond interactions with ASP220.

2.6. Molecular dynamic simulation (MDS)

Compound **4d** which showed the most favorable electrochemical profile was further studied for the binding interactions and the stability of the ligand-dsDNA complex in MDS studies. The plots of R_g versus time (ns) for the dsDNA was represented in **Fig. S43.** The R_g for dsDNA was noticed to have minimal fluctuations with consistency throughout the simulations which indicates the stability and rigidity of the system. The plot of RMSD versus time (ns) for the dsDNA and the ligand **4d** were represented in **Fig. S44-A** and **Fig. S44-B**, respectively. Even the RMSD values of dsDNA reached to 7 Å, after first 10 ns, the motions indicate the equilibrium since the changes were between 1 and 3 Å, and RMSD values of **4d** were 3.5 Å. which indicates that the conformational changes were in acceptable range [56] during the simulation.

The binding interactions of **4d** and dsDNA were also examined through MDS. As shown in Fig. 7, H-bonds, salt bridge, π–π stacking and π–cation interactions were all involved in the binding of the ligand and dsDNA. Also, in harmony with the previously mentioned docking results, A:DG4, DT7, DT19 and DC23 were among the important nucleotides that were involved in the binding interactions (**video 1**- Supplementary data). It has also been obsereved that the benzothiazole part of comound **4d** forms Ar H-bonds with DC23, DA5 and DG24 while the ortho substituted phenyl part forms Ar H-bonds with DT19 and DT20.

MDS studies of ligand **4d** within TS revealed that the value of protein RMSD changed by 2.7 Å which is within the acceptable range (1–3 Å), thus the protein has minimal conformation changes during the simulation. Additionally, the ligand RMSD (Fig. 8-B_L) was found to fluctuate by 2.3 Å, thus the ligand also has minimal internal changes, and it is stable with respect to the enzyme binding site. The RMSF values of the rigid protein structures (Fig. 8-B_R) showed minimal fluctations, moreover, the RMSF values of interacted loop amino acids found to fluctuate under 0.8 Å. Finally, the fractions, type and strength of the **4d**-TS interactions were represented in Fig. 8-C_L, Fig. 8-C_R and Fig. 8-E. A total number of twelve various interactions were made to the ligand **4d** by the protein during 100 nanoseconds simulation. These interactions include hydrophobic, H-bonds and water bridge interactions. The residues of Glu59, Asn228, Phe227 and Tyr145 were the main ones involved in the binding interactions, respectively. Additionally, the H_3 and H_4 of the phenyl group with ALA311, the H_5 of the phenyl group with Ile 80, the H_7 of the benzothiazolr ring with Leu223, the oxygen of the oxadiazole ring with Trp81 and the carbonyl of the amidic group with His198 were all noticed to be part of the involved Ar H-bonds (**video 2**- Supplementary data).

MDS studies were further performed for compound **4f** within the target DNA gyrase to evaluate the stability of the enzyme-ligand complex (Fig. 9-A, 9-B_L and 9-B_R), the ligand-enzyme contact (Fig. 9-C_L and 9-C_R) and the 2D enzyme-ligand interaction strengths (cut off 30%) (Fig. 10-E). As protein RMSD changes within the range of 1–3 Å are perfectly acceptable values for protein structures, the protein RMSD for compound **4f**-DNA gyrase (Fig. 9-B_L) was found to change by 2.5 Å which means that minimal conformation changes are observed for the protein during the simulation. Additionally, the ligand RMSD (Fig. 9-B_L) was found to change by 2 Å which means that minimal internal changes are observed within the ligand structure and the ligand **(4f)** is stable with respect to the enzyme binding site. For the protein RMSF (Fig. 9-B_R), the protein's secondary structures (α-helices and β-strands) showed lower fluctuations than the non-secondary structures (loop regions). The protein RMSF value of ligand **4f** was noticed to be stable. Finally, the strength, type and nature of the ligand **4f**-DNA gyrase interactions were represented in Fig. 9-C_L, 9-C_R and 9-E. During the 100 ns simulation, a total number of nine various interactions were made to the ligand **4f** by the protein including hydrophobic, H-bonds, ionic and water bridge interactions. The residues of D:ASP1083, B:ARG1122 and B:MET1121 were the main ones involved in the binding interactions, respectively. However, the Ar H-bonds include the interaction of the carbonyl of amidic group with Tyr 1087, H_5 and H_6 of the phenyl group with DA 2011 and the H_7 of benzothiazole with Asp 1083 (**video 3**- Supplementary data).

Generally, electrochemical and molecular mechanics studies point out that *N*-(benzothiazole-2-yl)acetamide moiety is favorable to dock to DNA minor grave, thereof, molecular mechanics studies predicted that

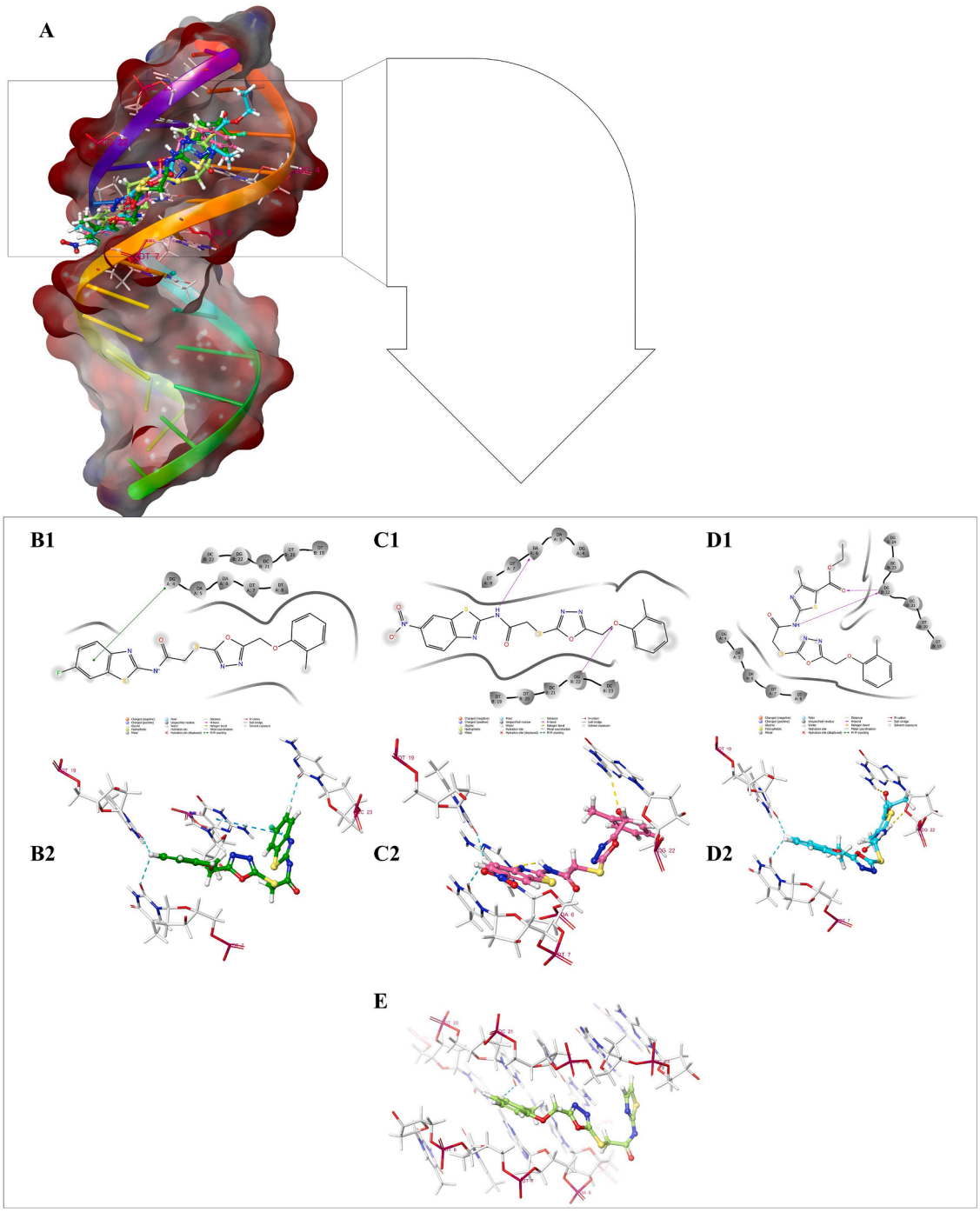

Fig. 5. Docking poses of active compounds with dsDNA. A: 3D Overlay poses of **4d, 4f, 4i** and **4h** within dsDNA. B1: and B2: 2D and 3D pose of **4d,** respectively. C1 and C2: 2D and 3D pose of **4f**, respectively. D1 and D2: 2D and 3D pose of **4i**, respectively. E: 3D pose of **4h**.

this compound has a potential to inhibit DNA-gyrase and TS enzymes. Moreover, the combination with the oxadiazole ring supported the TS inhibition as this ring interacted with Tyr145 amino acid, which is an important residue to stabilize the catalytic cavity of the enzyme [57].

On the other hand, 2-methyl phenoxy moiety can be simply said as managing the pharmacokinetic properties since it did not interact with important residues. Therefore, we suggested the following modifications to this phenoxy ring:

- Methyl substitution can be removed from the 2nd and added to the 4th position. Indeed, 2nd position of phenoxy should be empty to localize close to the loop region (Arg76-Trp81) of TS enzyme.
- Phenoxymethylene moiety should be here to obtain the rotation around itself.
- The phenoxy ring could be changed with nucleotides or their analogs to get better interaction with the DNA at DNA-gyrase active region, but oxymethylene residue should be protected.

3. Conclusions

In this study, ten *N*-(substituted benzothiazole/thiazol-2-yl)−2-((5-((o-tolyloxy)methyl)−1,3,4-oxadiazol-2-yl)thio)acetamide compounds were synthesized starting from *o*-cresol in four steps. *In-vitro* antibacterial and antifungal activity of these oxadiazole derivatives were

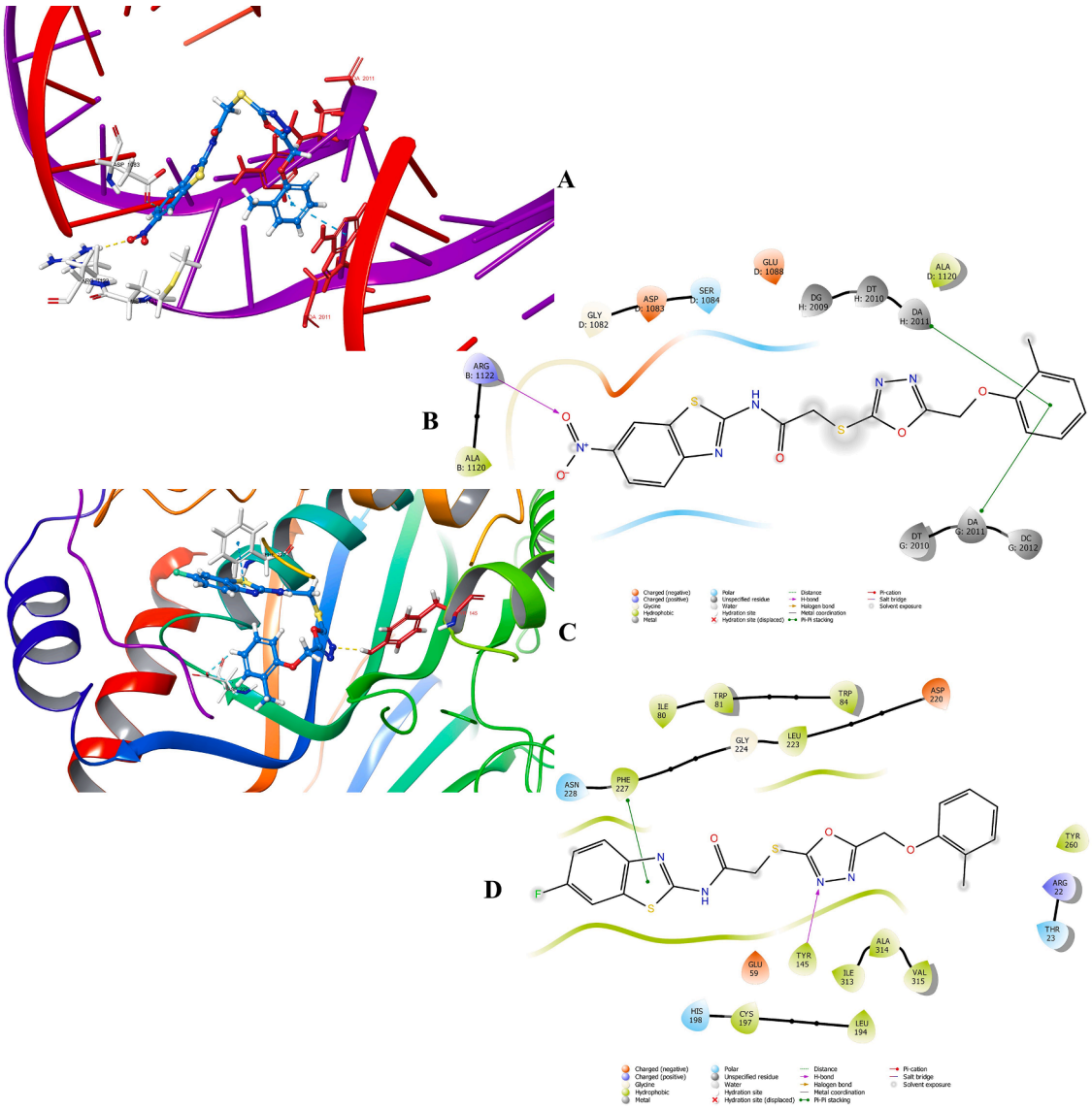

Fig. 6. Docking poses of compound **4f** within DNA gyrase (A and B) and compound **4d** within TS (C and D).

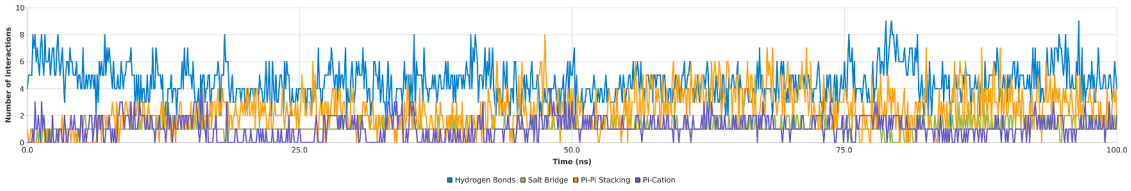

Fig. 7. The binding interactions of **4d** and dsDNA.

evaluated against several bacterial and candida species. The active compounds were evaluated for their activation mechanism using electrochemical and molecular mechanics techniques. The biological results indicated that *E. coli* and *E. faecalis* were the most susceptible bacterial strains, whereas *C. albicans* and *C. parapsilopsis* were the most vulnerable candidal pathogens. Compounds **4g** and **4i** were found to have considerable antibacterial and antifungal activity. Compounds **4f, 4d** and **4 h** also had a presumed antibacterial activity while **4j** exhibited a remarkable anticandidal effect. It was also found that the anticandidal activity of synthesized compounds is superior to antibacterial activity. The structure-activity relationship (with the *ds*DNA, DNA gyrase, and thymidylate synthase proteins) was explained by electrochemical method, molecular docking, and molecular dynamics simulation studies. According to all methods, we suggest 1,3,4-oxadiazole-(benzo)thiazole derivatives as potential antibacterial structures because they cause dsDNA poisoning by binding the guanine nucleotide. Based on expected ADME findings, these compounds might be orally bioavailable agents in the future. According to molecular *in silico* studies, 2-methyl phenoxy moiety is determined to improve the pharmacokinetic properties.

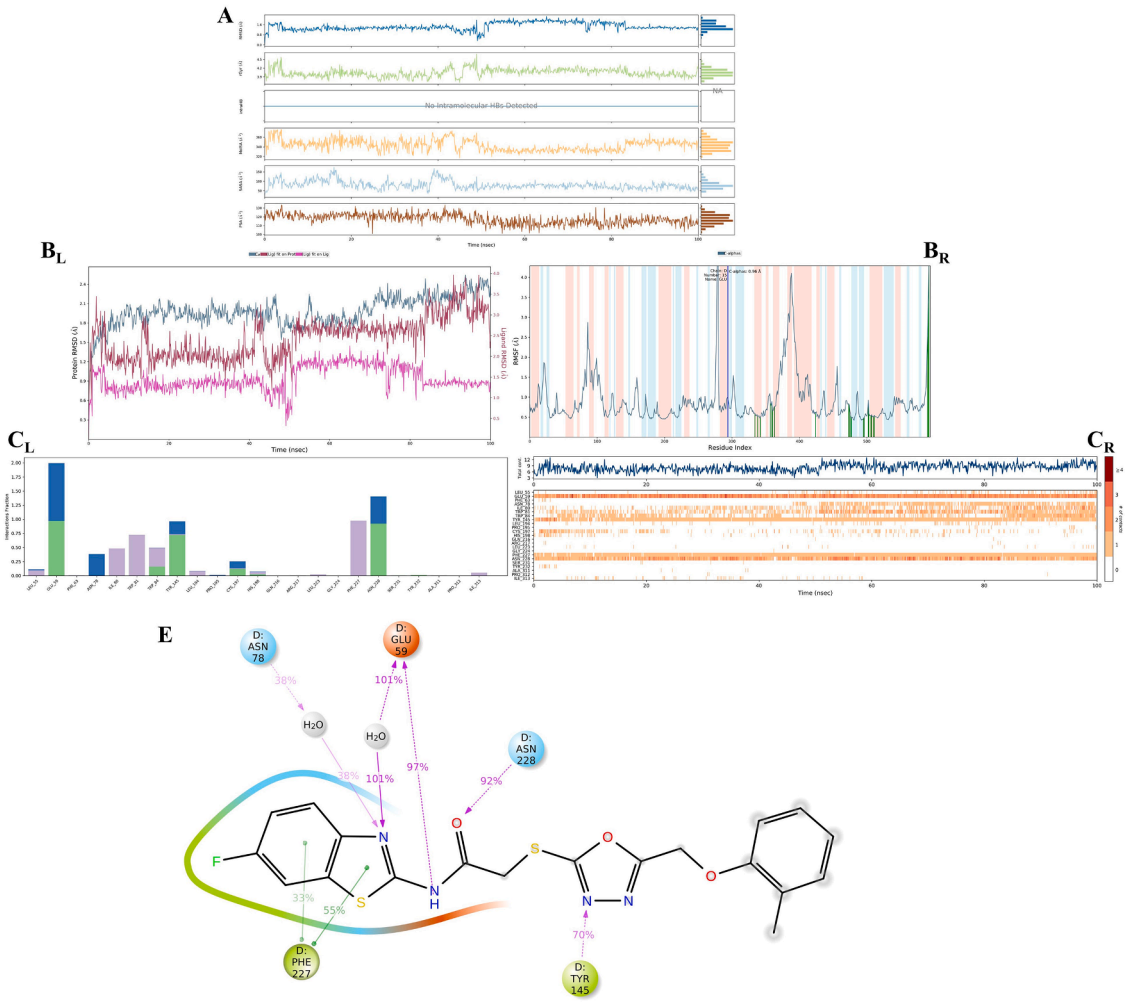

Fig. 8. MDS studies of ligand **4d** within TS. A:Physicochemical properties of the ligand, B_L: protein and ligand RMSD. B_R: Protein RMSF. C_L, C_R and E: the strength, type and nature of the ligand **4d**-TS interactions.

4. Materials and methods

4.1. Chemistry

All chemical substances were purchased from Sigma-Aldrich Chemical Co (Sigma-Aldrich Corp., St. Louis, MO, USA) and Merck Chemicals (Merck KGaA, Darmstadt, Germany). MP90 digital melting point apparatus (Mettler Toledo, Ohio, USA) was used to determine all melting points (m.p.) which were uncorrected. Using thin-layer chromatography (TLC), all reactions were monitored using Silica Gel 60 F_{254} TLC plates (Merck KGaA, Darmstadt, Germany). In TLC, petroleum ether-ethyl acetate (3:1) was used as a mobile phase. Spectroscopic data were recorded with the following instruments: Shimadzu-IR Affinity-IS instrument (Shimadzu, Japan); NMR, Bruker DPX-300 FT-NMR spectrometer (Bruker Bioscience, Billerica, MA, USA) and Bruker Ascend-400 NMR spectrometer (Bruker Bioscience, Billerica, MA, USA) in DMSO-d_6, using TMS as internal standard; Shimadzu 8040 LC/MS/MS system (Shimadzu, Tokyo, Japan) was used to determine $M+1$ peaks. Analysis data including IR, ^{1}H NMR, ^{13}C NMR and High-resolution mass spectra HRMS of all products are provided to supplement data.

4.1.1. General synthesis of ethyl 2-(o-tolyloxy)acetate (1)

Yield: 83%. An equimolar amount of both *o*-cresol (55.56 mmol, 6 g) and ethyl bromoacetate was refluxed in acetone and potassium carbonate K_2CO_3 for five hours. After the reaction was completed, the solvent was evaporated, and the product was washed with water before being filtered and recrystallized from ethanol.

4.1.2. General synthesis of 2-(o-tolyloxy)acetohydrazide (2)

Yield: 74%. Ethyl 2-(o-tolyloxy)acetate (28.35 mmol, 5.5 g) **(1)** was refluxed with an equivalent amount of hydrazine monohydrate in ethanol for seven hours. The product was filtered and recrystallized from ethanol.

4.1.3. General synthesis of 5-((o-tolyloxy)methyl)−1,3,4-oxadiazole-2-thiol (3)

Yield: 68%. 2-(o-Tolyloxy)acetohydrazide (18.86 mmol, 3.4 g) **(2)** was refluxed with an equivalent amount of carbon disulfide CS_2 for five hours in 2 N NaOH/EtOH solution. After the reaction was completed, it was cooled and neutralized in cold water with HCl. The precipitated product was filtered and washed with water.

4.1.4. General synthesis of 2,5-disubstituted 1,3,4- oxadiazole derivatives (4a-4j)

5-((o-Tolyloxy)methyl)−1,3,4-oxadiazole-2-thiol (1.35 mmol, 0.3 g) **(3)** were reacted with 1.35 mmol of 2-(2-chloroacetamide) benzothiazole differently substituted at the sixth position **(4a-g)** and 1.35 mmol of 2-[2-*chloroacetamide*]thiazole differently substituted at the fourth and fifth positions **(4h-j)** in acetone/K_2CO_3 at room temperature. Final products were dried from acetone, washed with water and recrystallized from ethanol.

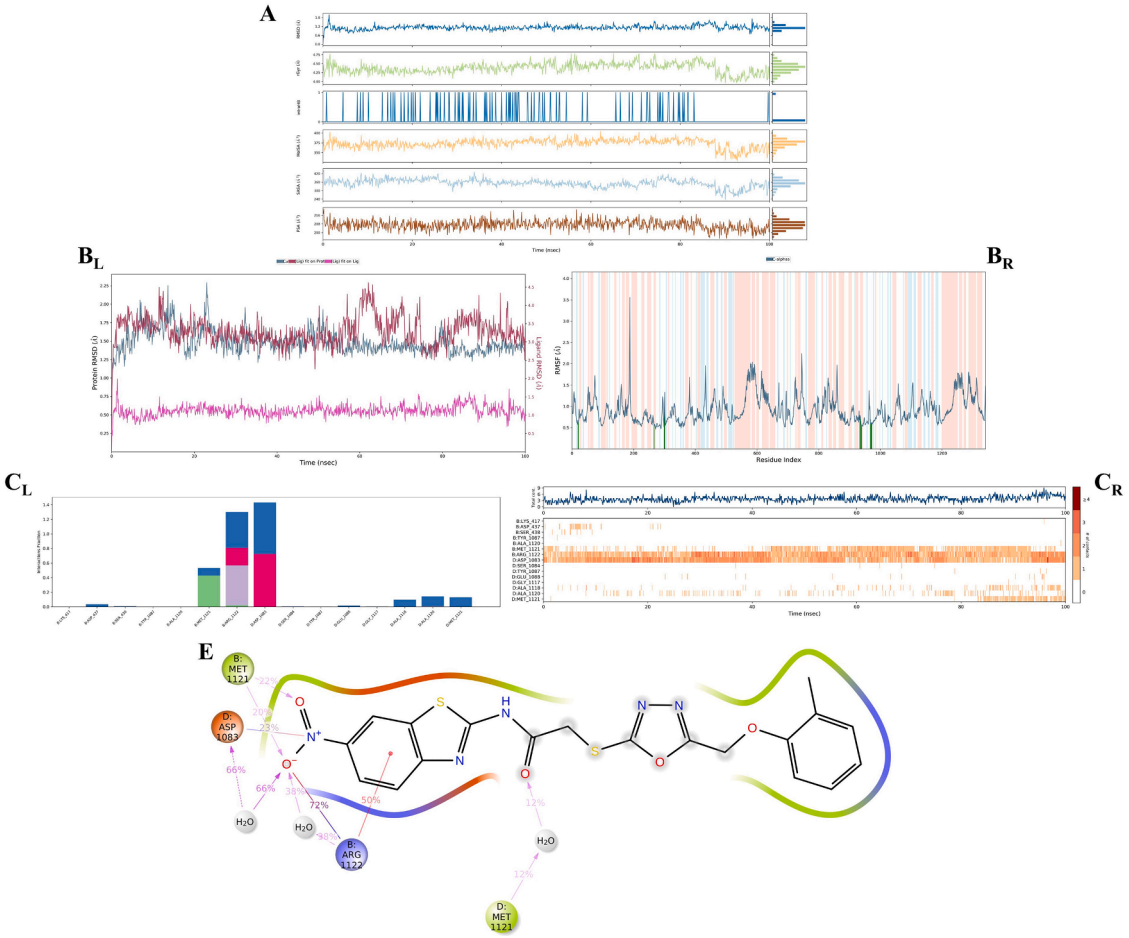

Fig. 9. MDS studies of ligand **4f** within DNA gyrase. A: Physicochemical properties of the ligand, B_L: protein and ligand RMSD. B_R: Protein RMSF. C_L, C_R and E: the strength, type and nature of the ligand **4f**- DNA gyrase interactions.

4.1.5. N-(benzo[d]thiazol-2-yl)−2-((5-((o-tolyloxy)methyl)−1,3,4-oxadiazol-2-yl)thio)acetamide (4a)

Yield: 78%. Melting point (m.p.): 216 °C. IR (ATR) υ_{max} (cm^{-1}): 3180 (N—H), 1686 (C=O), 1263–1032 (C—O). ^{1}H NMR (400 MHz, DMSO-d_6) δ: 2.12 (3H, s, -CH_3), 4.47 (2H, s, S –CH_2), 5.38 (2H, s, O—CH_2), 6.89 (1H, t, J = 7.29 Hz, Ar-H), 7.07 (1H, d, J = 8.02 Hz, Ar-H), 7.15 (2H, t, J = 9.06 Hz, Ar-H), 7.33 (1H, t, J = 7.52 Hz, benzothiazole H), 7.45 (1H, t, J = 7.61 Hz, benzothiazole H), 7.78 (1H, d, J = 8.06 Hz, benzothiazole-H_7), 7.99 (1H, d, J = 7.88 Hz, benzothiazole-H_4), 12.79 (1H, br s, NH). ^{13}C NMR (75 MHz, DMSO-d6): δ: 16.3 (CH_3), 36.6 (S-CH_2), 60.2 (O—CH_2), 112.7, 120.9, 122.1,122.1, 123.9, 126.5, 126.7, 127.5, 131.2, 132.0, 149.1, 155.8, 159.2, 164.4, 164.8, 167.1. HRMS (*m/z*): $[M+H]^+$ for $C_{19}H_{16}N_4O_3S_2$ calculated: 413.0737; found: 413.0724.

4.1.6. N-(6-methylbenzo[d]thiazol-2-yl)−2-((5-((o-tolyloxy)methyl)−1,3,4-oxadiazol-2-yl)thio)acetamide (4b)

Yield: 80%. M.p.: 227 °C. IR (ATR) υ_{max} (cm^{-1}): 3200 (N—H), 1690 (C=O), 1269–1028 (C—O). ^{1}H NMR (400 MHz, DMSO-d_6, ppm) δ: 2.11 (3H, s, Phenyl -CH_3), 2.41 (3H, s, benzothiazole-CH_3), 4.44 (2H, s, S –CH_2), 5.38 (2H, s, O—CH_2), 6.89 (1H, t, J = 7.18 Hz, Ar-H), 7.06 (1H, d, J = 7.82 Hz, Ar-H), 7.15 (2H, t, J = 7.97 Hz, Ar-H), 7.26 (1H, d, J = 8.20 Hz, benzothiazole H), 7.65 (1H, d, J = 8.17 Hz, benzothiazole H), 7.77 (1H, s, benzothiazole-H_7), 12.7 (1H, br s, NH).^{13}C NMR (75 MHz, DMSO-d_6, ppm) δ: 16.3 (Phenyl-CH_3), 21.64 (benzothiazole- CH_3), 36.1 (S-CH_2), 60.2 (O—CH_2), 112.7, 120.8, 121.8, 122.1, 127.5, 127.8, 128.0, 131.2, 133.2, 133.7, 155.8, 157.2, 157.3, 164.5, 164.8, 166.5. HRMS (*m/z*): $[M+H]^+$ for $C_{20}H_{18}N_4O_3S_2$ calculated: 427.0893; found: 427.0883.

4.1.7. N-(6-methoxybenzo[d]thiazol-2-yl)−2-((5-((o-tolyloxy)methyl)−1,3,4-oxadiazol-2-yl)thio)acetamide (4c)

Yield: 75%. M.p.: 221 °C. IR (ATR) υ_{max} (cm^{-1}): 3198 (N—H), 1690 (C=O), 1267–1028 (C—O). ^{1}H NMR (400 MHz, DMSO-d_6, ppm) δ: 2.12 (3H, s, Phenyl -CH_3), 3.81 (3H, s, O—CH_3), 4.44 (2H, s, S –CH_2), 5.38 (2H, s, O—CH_2), 6.89 (1H, t, J = 7.3 Hz, Ar-H), 7.06 (2H, t, J = 9.32 Hz, Ar-H), 7.15 (2H, t, J = 8.38 Hz, Ar-H), 7.58 (1H, s, benzothiazole-H_7), 7.66 (1H, d, J = 8.83 Hz, benzothiazole-H_4), 12.65 (1H, br s, NH). ^{13}C NMR (75 MHz, DMSO-d_6, ppm) δ: δ: 16.3 (Phenyl-CH_3), 36.2 (S-CH_2), 56.1 (benzothiazole- OCH_3), 60.2 (O—CH_2), 105.2, 112.7, 115.5, 121.7, 122.1, 126.7, 127.5, 131.2, 133.3, 143.0, 155.8, 156.5, 156.6, 164.5, 164.7, 166.5. HRMS (*m/z*): $[M+H]^+$ for $C_{20}H_{18}N_4O_4S_2$ calculated: 443.0842; found: 443.0839.

4.1.8. N-(6-fluorobenzo[d]thiazol-2-yl)−2-((5-((o-tolyloxy)methyl)−1,3,4-oxadiazol-2-yl)thio)acetamide (4d)

Yield: 75%. M.p.: 224 °C. IR (ATR) υ_{max} (cm^{-1}): 3198 (N—H), 1690 (C=O), 1246–1030 (C—O). ^{1}H NMR (400 MHz, DMSO-d_6, ppm) δ: 2.12 (3H, s, Phenyl -CH_3), 4.47 (2H, s, S –CH_2), 5.39 (2H, s, O—CH_2), 6.89 (1H, t, J = 7.19 Hz, Ar-H), 7.07 (1H, d, J = 7.9 Hz, Ar-H), 7.15 (2H, t, J = 9 Hz, Ar-H), 7.30 (1H, t, J = 8.95 Hz, Ar-H), 7.78 (1H, dd, J_1= 5.21 Hz, J_2= 8.76 Hz, benzothiazole-H), 7.9 (1H, d, J = 8.58 Hz, benzothiazole-H), 12.82 (1H, br s, NH). ^{13}C NMR (75 MHz, DMSO-d_6, ppm) δ: 16.3 (Phenyl-CH_3), 36.1 (S-CH_2), 60.2 (O—CH_2), 108.9, 112.7, 114.7, 122.1, 122.4, 126.7, 127.5, 131.2, 133.1, 145.7, 155.8, 157.6, 158.2, 160.8, 164.5, 166.8. HRMS (*m/z*): $[M+H]^+$ for $C_{19}H_{15}N_4O_3FS_2$ calculated: 431.0642; found: 431.0642.

4.1.9. N-(6-chlorobenzo[d]thiazol-2-yl)−2-((5-((o-tolyloxy)methyl)−1,3,4-oxadiazol-2-yl)thio)acetamide (4e)

Yield: 72%. M.p.: 250 °C. IR (ATR) υ_{max} (cm^{-1}): 3175 (N—H), 1694 (C=O), 1273–1036 (C—O). ^{1}H NMR (400 MHz, DMSO-d_6, ppm) δ: 2.11 (3H, s, Phenyl -CH_3), 4.45 (2H, s, S –CH_2), 5.37 (2H, s, O—CH_2), 6.89 (1H, t, J = 7.3 Hz, Ar-H), 7.06 (1H, d, J = 7.97 Hz, Ar-H), 7.15 (2H, t, J = 8.52 Hz, Ar-H), 7.46 (1H, d, J = 8.64 Hz, Ar-H), 7.76 (1H, d, J = 8.64 Hz, benzothiazole-H_4), 8.13 (1H, s, benzothiazole-H_7), 12.84 (1H, br s, NH).^{13}C NMR (100 MHz, DMSO-d_6, ppm) δ: 18.4 (Phenyl-CH_3), 36.1 (S-CH_2), 60.1 (O—CH_2), 112.8, 118.4, 122.1, 122.2, 127.5, 128.3, 131.2, 133.8, 159.3, 163.7. HRMS (*m/z*): $[M+H]^+$ for $C_{19}H_{15}N_4O_3ClS_2$ calculated: 447.0347; found: 447.0383.

4.1.10. N-(6-nitrobenzo[d]thiazol-2-yl)−2-((5-((o-tolyloxy)methyl)−1,3,4-oxadiazol-2-yl)thio)acetamide (4f)

Yield: 78%. M.p.: 225 °C. IR (ATR) υ_{max} (cm^{-1}): 3197 (N—H), 1686 (C=O), 1261–1029 (C—O). ^{1}H NMR (400 MHz, DMSO-d_6, ppm) δ: 2.12 (3H, s, Phenyl -CH_3), 4.47 (2H, s, S –CH_2), 5.39 (2H, s, O—CH_2), 6.89 (1H, t, J = 7.18 Hz, Ar-H), 7.07 (1H, d, J = 7.91 Hz, Ar-H), 7.15 (2H, t, J = 9.9 Hz, Ar-H), 7.87 (1H, d, J = 8.88 Hz, Ar-H), 8.26 (1H, d, J = 8.85 Hz, benzothiazole-H), 9.00 (1H, s, benzothiazole-H). ^{13}C NMR (75 MHz, DMSO-d_6, ppm) δ: 16.3 (Phenyl-CH_3), 37.4 (S-CH_2), 60.2 (O—CH_2), 112.7, 119.0, 120.4, 122.0, 122.1, 126.7, 127.5, 131.2, 133.0, 142.7, 154.8, 155.8, 164.3, 165.0, 166.7, 169.2. HRMS (*m/z*): $[M+H]^+$ for $C_{19}H_{15}N_5O_5S_2$ calculated: 458.0587; found: 458.0579.

4.1.11. N-(6-ethoxybenzo[d]thiazol-2-yl)−2-((5-((o-tolyloxy)methyl)−1,3,4-oxadiazol-2-yl)thio)acetamide (4g)

Yield: 75%. M.p.: 214 °C. IR (ATR) υ_{max} (cm^{-1}): 3180 (N—H), 1686 (C=O), 1263–1032 (C—O). ^{1}H NMR (400 MHz, DMSO-d_6, ppm) δ: 1.35 (3H, t, J = 6.83 Hz, OCH_2CH_3), 2.12 (3H, s, Phenyl -CH_3), 4.06 (2H, q, J_1= 6.82 Hz, J_2= 13.68 Hz, OCH_2CH_3), 4.44 (2H, s, S –CH_2), 5.38 (2H, s, O—CH_2), 6.89 (1H, t, J = 7.26 Hz, Ar-H), 7.03 (1H, d, J = 8.83 Hz, Ar-H), 7.07 (1H, d, J = 8.01 Hz, Ar-H), 7.15 (2H, t, J = 8.40 Hz, Ar-H), 7.55 (1H, s, Ar-H), 7.65 (1H, d, J = 8.79 Hz Ar-H), 12.65 (1H, br s, NH). ^{13}C NMR (75 MHz, DMSO-d_6, ppm) δ: 15.2 (benzothiazole-OCH_2CH_3), 16.3 (Phenyl-CH_3), 36.1 (S-CH_2), 60.2 (O—CH_2), 64.1 (benzothiazole-OCH_2CH_3), 105.8, 112.7, 115.9, 121.8, 122.1, 126.7, 127.5, 131.2, 133.2, 142.9, 155.8, 156.0, 164.5, 164.6, 166.3. HRMS (*m/z*): $[M+H]^+$ for $C_{21}H_{20}N_4O_4S_2$ calculated: 457.0999; found: 457.0985.

4.1.12. N-(thiazol-2-yl)−2-((5-((o-tolyloxy)methyl)−1,3,4-oxadiazol-2-yl)thio)acetamide (4h)

Yield: 80%. M.p.: 197 °C. IR (ATR) υ_{max} (cm^{-1}): 3198 (N—H), 1692 (C=O), 1242–1030 (C—O). ^{1}H NMR (400 MHz, DMSO-d_6, ppm) δ: 2.13 (3H, s, Phenyl -CH_3), 4.4 (2H, s, S –CH_2), 5.38 (2H, s, O—CH_2), 6.9 (1H, t, J = 7.29 Hz, Ar-H), 7.07 (1H, d, J = 8.26 Hz, Ar-H), 7.16 (2H, t, J = 6.84 Hz, Ar-H), 7.26 (1H, d, J = 3.06 Hz, Ar-H), 7.5 (1H, d, J = 3.08 Hz, Ar-H), 12.54 (1H, br s, NH). ^{13}C NMR (75 MHz, DMSO-d_6, ppm) δ: 16.3 (Phenyl-CH_3), 35.9 (S-CH_2), 60.2 (O—CH_2), 112.7, 114.3, 122.1, 126.7, 127.5, 131.2, 138.2, 155.8, 158.3, 164.5, 164.7, 165.6. HRMS (*m/z*): $[M+H]^+$ for $C_{15}H_{14}N_4O_3S_2$ calculated: 363.0580; found: 363.0568.

4.1.13. Ethyl-4-methyl-2-(2-((5-((o-tolyloxy)methyl)−1,3,4-oxadiazol-2-yl)thio)acetamido) thiazole-5-carboxylate (4i)

Yield: 77%. M.p.: 194 °C. IR (ATR) υ_{max} (cm^{-1}): 3172 (N—H), 1699 (C=O), 1263–1005 (C—O). ^{1}H NMR (400 MHz, DMSO-d_6, ppm) δ: 1.27 (3H, t, J = 7.04 Hz, OCH_2CH_3), 2.12 (3H, s, Phenyl -CH_3), 2.55 (3H, s, thiazole-CH_3), 4.24 (2H, q, J_1= 7.03 Hz, J_2= 14.1 Hz, OCH_2CH_3), 4.4 (2H, s, S –CH_2), 5.37 (2H, s, O—CH_2), 6.9 (1H, t, J = 7.27 Hz, Ar-H), 7.06 (1H, d, J = 8.02 Hz, Ar-H), 7.16 (2H, d, J = 7.66 Hz, Ar-H), 12.98 (1H, br s, NH). ^{13}C NMR (75 MHz, DMSO-d_6, ppm) δ: 14.6 (OCH_2CH_3), 16.28 (Phenyl-CH_3), 17.46 (thiazole-CH_3), 36.14 (S-CH_2), 60.17 (O—CH_2), 60.95 (OCH_2CH_3), 112.7, 114.5, 122.1, 126.7, 127.5, 131.2, 155.8, 156.7, 160.4, 162.5, 164.5, 164.6, 166.9. HRMS (*m/z*): $[M+H]^+$ for $C_{19}H_{20}N_4O_5S_2$ calculated: 449.0948; found: 449.0930.

4.1.14. Ethyl-2-(2-(2-((5-((o-tolyloxy)methyl)−1,3,4-oxadiazol-2-yl)thio)acetamido)thiazol-4-yl)acetate (4j)

Yield: 70%. M.p.: 134 °C. IR (ATR) υ_{max} (cm^{-1}): 3173 (N—H), 1738 (C=O), 1666 (C=O), 1240–1028 (C—O). ^{1}H NMR (300 MHz, DMSO-d_6, ppm) δ: 1.17 (3H, t, J = 7.1 Hz, OCH_2CH_3), 2.12 (3H, s, Phenyl -CH_3), 3.67 (2H, s, thiazole-CH_2), 4.07 (2H, q, J_1= 7.09 Hz, J_2= 14.19 Hz, OCH_2CH_3), 4.33 (2H, s, S –CH_2), 5.37 (2H, s, O—CH_2), 6.89 (1H, t, J = 7.28 Hz, Ar-H), 6.95 (1H, s, Ar-H), 7.06 (1H, d, J = 8.5 Hz, Ar-H), 7.14 (2H, d, J = 7.07 Hz, Ar-H), 12.63 (1H, br s, NH). ^{13}C NMR (75 MHz, DMSO-d_6, ppm) δ: 14.6 (OCH_2CH_3), 16.3 (Phenyl-CH_3), 36.3 (S-CH_2), 37.2 (thiazole- CH_2) 60.2 (O—CH_2), 60.8 (OCH_2CH_3), 110.9, 112.7, 122.1, 126.7, 127.5, 131.2, 144.1, 155.8, 159.0, 164.4, 164.8, 165.9, 170.5. HRMS (*m/z*): $[M+H]^+$ for $C_{19}H_{20}N_4O_5S_2$ calculated: 449.0948; found: 449.0927.

4.2. Antimicrobial activity

The antimicrobial activity of the compounds was tested on microorganisms *E. coli* (ATCC 25,922), *S. marcescens* (ATCC 8100), *K. pneumoniae* (ATCC 13,883), *P. aeruginosa* (ATCC 27,853), *E. faecalis* (ATCC 2942), *B. subtilis* (ATCC), *S. aureus* (ATCC 29,213) and *S. epidermidis* (ATCC 12,228) as bacteria; *C. albicans* (ATCC 24,433), *C. krusei* (ATCC 6258) and *C. parapsilopsis* (ATCC 22,019) as yeasts. To maintain bacterial cultures, Mueller-Hinton agar (MHA) plates were introduced, whereas sabourad dextrose agar (SDA) was used to maintain fungal cultures. The Minimum Inhibition Concentration (MIC) tests using 96-well microplates were performed by the microdilution standard methods CLSI M07-A9 (2012) [58] and NCCLS M27-A2 (2002) [59] for bacteria and yeasts, respectively. Mueller-Hinton broth (MHB) for bacteria and sabourad dextrose broth (SDB) media were used for the growth of test microorganisms in the antimicrobial experiments. The wells were prepared to contain 100 µl volume in the final case. Using 1000 ppm stock solutions, each compound concentration in the first well was prepared to be 250 µg/ml. Serial dilutions were made in a 1: 2 ratio and the concentrations of the next wells were adjusted to 125, 62.5, 31.25, 15.625, 7.81, 3.90, 1.95, and 0.97 µg/ml, respectively. The microbial suspension adjusted to a 0.5 Mc Farland standard was inoculated into wells. The bacteria and yeasts were incubated for 24 h at 37 °C and 48 h at 35 °C, respectively. The same procedures were applied to Azithromycin for bacteria as the positive control. Voriconazole and Fluconazole were used as the positive control for yeast cells. Negative controls contained only dilute solutions without microorganisms. Positive and negative results were evaluated according to turbidity that occurred after 24–48 h by comparing them to the ones in the control wells. The lowest concentrations giving no visible growth for each microorganism were defined as MIC. The turbidity showing microbial growth after incubation was measured at OD600 nm wavelength with a multi-well plate reader (Multiskan FC, Thermo Scientific, Massachusetts, USA). All the chemicals used in the experiments were purchased from Merck. All antimicrobial studies were carried out triplicated with aseptic conditions.

4.3. Electrochemical studies

Apparatus: Both voltammetric and impedimetric measurements were performed by IVIUM Compactstat.e with IVIUM Release 4.951 software package (Holland). Pencil graphite electrode (PGE) was used as the disposable electrode material to monitor the interaction processes occurred the compounds and dsDNA. PGE consisted of a graphite lead (TOMBOW, 0.5, Japan) and a pencil (Rotring, Germany) soldered by a metallic wire to provide electrically conductive body. The PGE was a part of three-electrochemical cell system which included a working electrode (PGE), a reference electrode (Ag/AgCl/3 M KCl), and a counter electrode (Pt wire). For each measurement, 10 mm of a graphite lead should have been into the measurement solution.

Chemicals: Double stranded fish sperm DNA (dsDNA), trizma

hydrochloride ($NH_2C(CH_2OH)_3$·HCl), potassiumhexacyanoferrate(II) trihydrate ($K_4Fe(CN)_6$·$3H_2O$), potassiumhexacyanoferrate(III) ($K_3Fe(CN)_6$), potassium chloride (KCl), sodium chloride (NaCl), di-potassiumhydrogen phosphate (K_2HPO_4), ethylenediaminetetraacetic-acid disodium salt dihydrate ($C_{10}H_{14}N_2Na_2O_8$·$2H_2O$), potassiumdihydrogen phosphate (KH_2PO_4), and acetic acid (CH_3CO_2H) were purchased from Sigma-Aldrich (Sigma-Aldrich Corp., St. Louis, MO, USA). Tris-EDTA buffer solution containing 10 mM Tris- HCl and 1 mM EDTA (pH 8.00) was used to prepare 1000 μg/mL DNA stock solution. The stock solution was kept frozen. All chemicals were of analytical reagent grade and were purchased from Sigma-Aldrich and Merck. All buffer solutions were prepared in ultrapure water purchased from Bilecik Seyh Edebali University Central Research and Application Laboratory.

Preparation of dsDNA modified PGEs: The disposable PGEs electrochemically pretreated by applying +1.40 V potential during 30 s in acetate buffer solution (0.50 M acetate buffer containing 20 mM NaCl, ABS, pH 4.80). The dsDNA solution was diluted in ABS (pH 4.80) at 30 μg/mL concentration level since this concentration level was optimized in our previous report [60]. Then, each PGE was dipped into 100 μL of dsDNA solution during 15 mins. The dsDNA modified electrodes were gently immersed into ABS (pH 4.80) to eliminate unspecific binding of dsDNA molecules. Finally, dsDNA modified PGEs were ready to use in further experimental steps.

Interaction between the compounds and dsDNA at the surface of the PGEs: 0.95 μg/Ml of compounds **4d** and **4f** while 1.95 μg/mL of compounds **4h** and **4i** were prepared in 50 mM phosphate buffer solution (PBS, pH 7.40). These concentrations were their MIC levels. dsDNA modified PGEs were immersed into 100 μL of the compound solution. For the investigation of the effect of interaction time, dsDNA modified PGEs were incubated in the compound solution during 5, 15, 30 or 60 min. For empedimetric studies, 15 min interaction time was used. After all interaction processes, the PGEs were washed in PBS (pH 7.40) during 5 s. All PGEs were ready for electrochemical measurements.

Electrochemical measurements:

Differential pulse voltammetry (DPV) measurements: Voltammetric measurements were done in ABS (pH 4.80) between the potential of +0.60 V and +1.20 V at a pulse amplitude of 50 mV and scan rate of 50 mV/s.

Electrochemical impedance spectroscopy (EIS) measurements: A redox probe containing 2.50 mM $K_3[Fe(CN)_6]/K_4[Fe(CN)_6]$ (1:1) and 0.10 M KCl was used for all impedimetric measurements. Before and after each modification/interaction process, the measurements were performed in the frequency range from 100 mHz to 100 kHz at a potential of + 0.23 V with a sinusoidal signal of 10 mV. The frequency interval divided into 98 logarithmically equidistant measure points. The impedimetric data were fitted by Randles circuit was the equivalent circuit consisted of R_{ct} (the respective semicircle diameter corresponds to the charge-transfer resistance that occurred at the electrode-electrolyte interface), R_s (the solution resistance), Q (the capacitance related to the space charge capacitance between the electrode-electrolyte interface), and W (Warburg impedance due to mass transfer to the electrode surface). All experiments were done at room temperature.

4.4. ADME parameters

Early prediction of the pharmacokinetic profile is a necessity during drug development process to avoid later stages drug failures [61]. Molsoft software [53] and the SwissADME [54] program were used to compute the ADME properties of the target compounds **4a-4j**.

4.5. Molecular docking

Molecular docking studies of the most active compounds were applied to define their binding patterns within the related active sites using the *in silico* Schrödinger Maestro interface [62]. The X-ray crystal structures of dsDNA (PDB ID: 4AGZ), DNA gyrase (PDB ID: 6Z1A) [63] and thymidylate synthase (TS) of *Enterococcus faecalis* (PDB ID: 5J7W) [64] were imported from the Protein Data Bank server (www.rcsb.org). The Protein Preparation Wizard protocol of the Schrödinger Suite 2020 was then used to build the structure of the enzymes. The protonation states as well as the atom types were assigned using the LigPrep module [65] in order to prepare the ligands. Besides that, bond orders and hydrogen atoms were added to the structures. The Glide module [66] was applied for grid generation while docking runs were all optimized by using the standard precision docking mode.

4.6. Molecular dynamic simulation (MDS)

MDS studies were applied to evaluate the time-dependent stability of a ligand-target complex. The Desmond program [67] was applied by using the standard force field (OPLS3e) of the Schrödinger Suite with a transferable intermolecular potential with a 3-points (TIP3P) water model followed by energy minimization of the complex [68]. The system was neutralized by utilizing Na^+ and Cl^- ions. After the system setup was completed, MDS studies were performed. The MDS studies were recorded for 100 ns and the radius of gyration (R_g), root square deviations (RMSD) and root-mean-square fluctuation (RMSD) values were all calculated by the Desmond program [67].

CRediT authorship contribution statement

Amal A. AL-Sharabi: Conceptualization, Methodology, Formal analysis, Investigation, Data curation, Writing – original draft, Writing – review & editing, Visualization. **Sana Saffour:** Methodology, Formal analysis, Investigation, Writing – original draft, Visualization. **Asaf Evrim Evren:** Conceptualization, Methodology, Software, Investigation, Writing – review & editing, Visualization, Supervision. **Gizem Bayazıt:** Methodology, Formal analysis, Investigation, Writing – original draft, Writing – review & editing. **Gülşah Çongur:** Methodology, Formal analysis, Investigation, Writing – original draft, Writing – review & editing, Visualization. **Ülküye Dudu Gül:** Methodology, Formal analysis, Investigation, Writing – original draft, Writing – review & editing. **Leyla Yurttaş:** Conceptualization, Investigation, Resources, Data curation, Writing – review & editing, Visualization, Supervision.

Declaration of Competing Interest

The authors declare that they have no known competing financial interests or personal relationships that could have appeared to influence the work reported in this paper. e

Data availability

No data was used for the research described in the article.

Acknowledgments

None.

Supplementary materials

Supplementary material associated with this article can be found, in the online version, at doi:10.1016/j.molstruc.2023.135775.

References

[1] P. Dadgostar, Antimicrobial resistance: implications and costs, Infect. Drug Resist. (2019) 3903–3910.
[2] World Health Organization. (2021). Global antimicrobial resistance and use surveillance system (GLASS) report: 2021.

[3] M. Fesatidou, A. Petrou, G. Athina, Heterocycle compounds with antimicrobial activity, Curr. Pharm. Des. 26 (8) (2020) 867–904.
[4] T. Glomb, P. Swiatek, Antimicrobial activity of 1,3,4-oxadiazole derivatives, Int. J. Mol. Sci. 22 (13) (2021).
[5] E. Jafari, T. Mohammadi, A. Jahanian-Najafabadi, F. Hassanzadeh, Synthesis and antimicrobial evaluation of some 2,5 disubstituted 1,3,4-oxadiazole derivatives, Res. Pharm. Sci. 12 (4) (2017) 330–336.
[6] G. Naganagowda, A. Petsom, Synthesis and antimicrobial activity of some new 5-(3-chloro-1-benzothiophen-2-YL)-1,3,4-oxadiazole-2-thiol and their derivatives, Phosphorus Sulfur Silicon Relat. Elem. 186 (10) (2011) 2112–2121.
[7] R. Aziz ur, S. Gul, M.A. Abbasi, K. Nafeesa, M.N. Akhtar, I. Ahmad, S. Afzal, Synthesis, structural analysis, and screening of some novel 5-substituted aryl/aralkyl-1,3,4-oxadiazol-2-yl 4-(morpholin-4-ylsulfonyl)benzyl sulfides as potential antibacterial agents, Phosphorus Sulfur Silicon Relat. Elem. 190 (7) (2015) 1045–1055.
[8] T. Karabasanagouda, A.V. Adhikari, N.S. Shetty, Synthesis and antimicrobial activities of some novel 1,3,4-oxadiazoles carrying alkylthio and alkylsulphonyl phenoxy moieties, Phosphorus Sulfur Silicon Relat. Elem. 182 (12) (2007) 2925–2941.
[9] M.J. Ahsan, J.G. Samy, H. Khalilullah, M.S. Nomani, P. Saraswat, R. Gaur, A. Singh, Molecular properties prediction and synthesis of novel 1,3,4-oxadiazole analogues as potent antimicrobial and antitubercular agents, Bioorg. Med. Chem. Lett. 21 (24) (2011) 7246–7250.
[10] N.C. Desai, A.M. Dodiya, K.M. Rajpara, Y.M. Rupala, Synthesis and antimicrobial screening of 1,3,4-oxadiazole and clubbed thiophene derivatives, J. Saudi Chem. Soc. 18 (3) (2014) 255–261.
[11] A. M. Salahuddin, M.S. Yar, R. Mazumder, G.S. Chakraborthy, M.J. Ahsan, M. U. Rahman, Updates on synthesis and biological activities of 1,3,4-oxadiazole: a review Synth. Commun. 47 (20) (2017) 1805–1847.
[12] H. Khalilullah, M.J. Ahsan, M. Hedaitullah, S. Khan, B. Ahmed, 1,3,4-oxadiazole: a biologically active scaffold, Mini Rev. Med. Chem. 12 (8) (2012) 789–801.
[13] G. Verma, M.F. Khan, W. Akhtar, M.M. Alam, M. Akhter, M. Shaquiquzzaman, A review exploring therapeutic worth of 1,3,4-oxadiazole tailored compounds, Mini Rev. Med. Chem. 19 (6) (2019) 477–509.
[14] A. Siwach, P.K. Verma, Therapeutic potential of oxadiazole or furadiazole containing compounds, BMC Chem. 14 (1) (2020) 70.
[15] S. Nayak, S.L. Gaonkar, A review on recent synthetic strategies and pharmacological importance of 1, 3-thiazole derivatives, Mini Rev. Med. Chem. 19 (3) (2019) 215–238.
[16] S.H. Ali, A.R. Sayed, Review of the synthesis and biological activity of thiazoles, Synth. Commun. 51 (5) (2021) 670–700.
[17] D. Sharma, K.K. Bansal, A. Sharma, M. Pathak, P.C. Sharma, A brief literature and review of patents on thiazole related derivatives, Curr. Bioact. Compd. 15 (3) (2019) 304–315.
[18] S. Agarwal, D. Gandhi, P. Kalal, Benzothiazole: a versatile and multitargeted pharmacophore in the field of medicinal chemistry, Lett. Org. Chem. 14 (10) (2017) 729–742.
[19] S. Choudhary, G. Jeyabalan, N. Kalra, Review: therapeutic and biological activity of benzothiazole derivatives, Int. J. Recent Adv. Sci. Technol. 4 (2017) 8–20.
[20] M. Bhat, S.L. Belagali, Structural activity relationship and importance of benzothiazole derivatives in medicinal chemistry: a comprehensive review, Mini Rev. Org. Chem. 17 (3) (2020) 323–350.
[21] A. Rouf, C. Tanyeli, Bioactive thiazole and benzothiazole derivatives, Eur. J. Med. Chem. 97 (2015) 911–927.
[22] A. Qureshi, A. Pradhan, Short review on thiazole derivative, J. Drug Deliv. Ther. 9 (4–A) (2019) 842–847.
[23] I. Mishra, R. Mishra, S. Mujwar, P. Chandra, N. Sachan, A retrospect on antimicrobial potential of thiazole scaffold, J. Heterocycl. Chem. 57 (6) (2020) 2304–2329.
[24] A. Kashyap, N. Adhikari, A. Das, A. Shakya, S.K. Ghosh, U.P. Singh, H.R. Bhat, Review on synthetic chemistry and antibacterial importance of thiazole derivatives, Curr. Drug Discov. Technol. 15 (3) (2018) 214–228.
[25] M. Gjorgjieva, T. Tomašič, D. Kikelj, L.P. Mašič, Benzothiazole-based compounds in antibacterial drug discovery, Curr. Med. Chem. 25 (38) (2018) 5218–5236.
[26] M. T Chhabria, S. Patel, P. Modi, P. S Brahmkshatriya, Thiazole: a review on chemistry, synthesis and therapeutic importance of its derivatives, Curr. Top. Med. Chem. 16 (26) (2016) 2841–2862.
[27] M. Asif, M. Imran, A mini-review on pharmacological importance of benzothiazole scaffold, Mini Rev. Org. Chem. 18 (8) (2021) 1086–1097.
[28] I. Ali, S.D. Mukhtar, M.F. Hsieh, Z.A. Alothman, A. Alwarthan, Facile synthesis of indole heterocyclic compounds based micellar nano anti-cancer drugs, RSC Adv. 8 (66) (2018) 37905–37914.
[29] M.N. Patel, P.S. Karia, P.A. Vekariya, A.P. Patidar, Synthesis of heterocyclic compounds and its applications, Arab. J. Chem. 12 (8) (2019) 2983–2991.
[30] R. Ashraf, M.A. Iqbal, H.N. Bhatti, M.R.S.A. Janjua, M. El-Naggar, Bioactivity and DNA/BSA interactions of selenium N-heterocyclic carbene adducts, ChemistrySelect 5 (35) (2020) 10970–10981.
[31] S. Harlepp, E. Chardon, M. Bouché, G. Dahm, M. Maaloum, S. Bellemin-Laponnaz, N-Heterocyclic carbene-platinum complexes featuring an anthracenyl moiety: anti-cancer activity and DNA interaction, Int. J. Mol. Sci. 20 (17) (2019) 4198.
[32] V. Sharma, M. Gupta, P. Kumar, A. Sharma, A Comprehensive review on fused heterocyclic as DNA intercalators: promising anticancer agents, Curr. Pharm. Des. 27 (1) (2021) 15–42.
[33] M. Hasanzadeh, N. Shadjou, Pharmacogenomic study using bio-and nanobioelectrochemistry: drug–DNA interaction, Mater. Sci. Eng. C 61 (2016) 1002–1017.
[34] H. He, W. Wang, Y. Zhou, Q. Xia, Y. Ren, J. Feng, H. Peng, H. He, L. Feng, Rational design, synthesis and biological evaluation of 1, 3, 4-oxadiazole pyrimidine derivatives as novel pyruvate dehydrogenase complex E1 inhibitors, Bioorg. Med. Chem. 24 (8) (2016) 1879–1888.
[35] P. Kaur, Z.R. Bhat, S. Bhat, R. Kumar, R. Kumar, K. Tikoo, J. Gupta, N. Khurana, J. Kaur, G.L. Khatik, Synthesis and evaluation of new 1, 2, 4-oxadiazole based trans-acrylic acid derivatives as potential PPAR-alpha/gamma dual agonist, Bioorg. Chem. 100 (2020), 103867.
[36] N. Kulabaş, A. Türe, A. Bozdeveci, V.S. Krishna, Ş. Alpay Karaoğlu, D. Sriram, İ. Küçükgüzel, Novel fluoroquinolones containing 2-arylamino-2-oxoethyl fragment: design, synthesis, evaluation of antibacterial and antituberculosis activities and molecular modeling studies, J. Heterocycl. Chem. 59 (5) (2022) 909–926.
[37] S.K. Suthar, N.S. Chundawat, G. Pal Singh, J. M. Padrón, P.V. Payghan, Y.K. Jhala, Evaluation of anti-bacterial activity of novel 2, 3-diaminoquinoxaline derivatives: design, synthesis, biological screening, and molecular modeling studies, Egypt. J. Basic Appl. Sci. 9 (1) (2022) 162–179.
[38] S.N. Dighe, T.A. Collet, Recent advances in DNA gyrase-targeted antimicrobial agents, Eur. J. Med. Chem. 199 (2020), 112326.
[39] N.G.I. Biteau, Synthèse D'acyclonucléotides Et Hétérocycles Visant L'inhibition De La Thymidylate Synthase Flavine-Dépendante, Université d'Orléans, 2019.
[40] Z.M.M. Alzhrani, M.M. Alam, T. Neamatallah, S. Nazreen, Design, synthesis and *in vitro* antiproliferative activity of new thiazolidinedione-1, 3, 4-oxadiazole hybrids as thymidylate synthase inhibitors, J. Enzyme Inhib. Med. Chem. 35 (1) (2020) 1116–1123.
[41] S. Agnello, M. Brand, M.F. Chellat, S. Gazzola, R. Riedl, A structural view on medicinal chemistry strategies against drug resistance, Angew. Chem. Int. Ed. 58 (11) (2019) 3300–3345.
[42] M.M. Alam, A.S. Almalki, T. Neamatallah, N.M. Ali, A.M. Malebari, S. Nazreen, Synthesis of new 1, 3, 4-oxadiazole-incorporated 1, 2, 3-triazole moieties as potential anticancer agents targeting thymidylate synthase and their docking studies, Pharmaceuticals 13 (11) (2020) 390.
[43] F.A. Omar, M. Abelrasoul, M.M. Sheha, H.Y. Hassan, Y.M. Ibrahiem, Synthesis, antibacterial activity and molecular docking of substituted naphthyridines as potential DNA gyrase inhibitors, ChemistrySelect 3 (9) (2018) 2604–2612.
[44] Cruz De la, K. Morales, G. Alarcón-Angeles, A. Merkoçi, Nanomaterial-based sensors for the study of DNA interaction with drugs, Electroanalysis 31 (10) (2019) 1845–1867.
[45] P.A.V. de Carvalho, I.C. Lopes, E.H.C. Silva, E.E.S. Bruzaca, H.J. Alves, M.I.S. Lima, A.A. Tanaka, Electrochemical behaviour of anticancer drug lomustine and in situ evaluation of its interaction with DNA, J. Pharm. Biomed. Anal. 176 (2019), 112786.
[46] E.E.S. Bruzaca, I.C. Lopes, E.H.C. Silva, P.A.V. Carvalho, A.A. Tanaka, Electrochemical oxidation of the antitumor antibiotic mitomycin C and in situ evaluation of its interaction with DNA using a DNA-electrochemical biosensor, Microchem. J. 133 (2017) 81–89.
[47] G. Paimard, M.B. Gholivand, M. Shamsipur, Determination of ganciclovir as an antiviral drug and its interaction with DNA at Fe3O4/carboxylated multi-walled carbon nanotubes modified glassy carbon electrode, Measurement 77 (2016) 269–277.
[48] E.E. Salama, Synthesis of new 2-amino-1, 3, 4-oxadiazole derivatives with anti-salmonella typhi activity evaluation, BMC chem. 14 (1) (2020) 1–8.
[49] T. Akhtar, S. Hameed, N. A AL-MASOUDI, r. loddo, P. La Colla, *In vitro* antitumor and antiviral activities of new benzothiazole and 1, 3, 4-oxadiazole-2-thione derivatives, Acta Pharm. 58 (2) (2008) 135–149.
[50] T. Bal-Demirci, G. Congur, A. Erdem, S. Erdem-Kuruca, N. Özdemir, K. Akgün-Dar, B. Varol, B. Ülküseven, Iron (III) and nickel (II) complexes as potential anticancer agents: synthesis, physicochemical and structural properties, cytotoxic activity and DNA interactions, New J. Chem. 39 (7) (2015) 5643–5653.
[51] G. Congur, A. Erdem, F. Mese, Electrochemical investigation of the interaction between topotecan and DNA at disposable graphite electrodes, Bioelectrochemistry 102 (2015) 21–28.
[52] G. Congur, E. Eksin, A. Erdem, Levan modified DNA biosensor for voltammetric detection of daunorubicin-DNA interaction, Sens. Actuators B Chem. 326 (2021), 128818.
[53] L.L.C.M. Drug-Likeness and molecular property prediction.Molsoft: https://molsoft.com/mprop/, last accessed 15 Dec 2022.
[54] A. Daina, O. Michielin, V. Zoete, SwissADME: a free web tool to evaluate pharmacokinetics, drug-likeness and medicinal chemistry friendliness of small molecules, Sci. Rep. 7 (2017) 42717.
[55] R.M. van Harten, R.J.L. Willems, N.I. Martin, A.P.A. Hendrickx, Multidrug-resistant enterococcal infections: new compounds, novel antimicrobial therapies? Trends Microbiol. 25 (6) (2017) 467–479.
[56] D. Osmaniye, A.E. Evren, Ş. Karaca, Y. Özkay, Z.A. Kaplancıklı, Novel thiadiazol derivatives; design, synthesis, biological activity, molecular docking and molecular dynamics, J. Mol. Struct. (2023) 1272.
[57] C. Pozzi, S. Ferrari, R. Luciani, G. Tassone, M.P. Costi, S. Mangani, Structural comparison of enterococcus faecalis and human thymidylate synthase complexes with the substrate dUMP and its analogue FdUMP provides hints about enzyme conformational variabilities, Molecules 24 (7) (2019) 1257.
[58] Clinical, Institute, L.S., Methods For Dilution Antimicrobial Susceptibility Tests For Bacteria That Grow aerobically; Approved Standard, Clinical and Laboratory Standards Institute Wayne, PA, 2012.
[59] Wayne, P.A. (2002). Reference method for broth dilution antifungal susceptibility testing of yeasts, approved standard. *CLSI document M27-A2*.

[60] G. Çongur, Electrochemical investigation of the interaction of 2, 4-D and double stranded DNA using pencil graphite electrodes, TUrk. J. Chem. 45 (3) (2021) 600–615.
[61] H. van de Waterbeemd, E. Gifford, ADMET in silico modelling: towards prediction paradise? Nat. Rev. Drug Discov. 2 (3) (2003) 192–204.
[62] Maestro (2020). Schrödinger, Schrödinger Release 2020-3. New York, NY: Schrödinger, LLC. https://www.schrodinger.com/products/ maestro.
[63] A. Kolaric, T. Germe, M. Hrast, C.E.M. Stevenson, D.M. Lawson, N.P. Burton, J. Voros, A. Maxwell, N. Minovski, M. Anderluh, Potent DNA gyrase inhibitors bind asymmetrically to their target using symmetrical bifurcated halogen bonds, Nat. Commun. 12 (1) (2021) 150.
[64] A. Catalano, R. Luciani, A. Carocci, D. Cortesi, C. Pozzi, C. Borsari, S. Ferrari, S. Mangani, X-ray crystal structures of Enterococcus faecalis thymidylate synthase with folate binding site inhibitors, Eur. J. Med. Chem. 123 (2016) 649–664.
[65] LigPrep (2020). Schrödinger, Schrödinger Release 2020-3. New York, NY: Schrödinger, LLC. https://www.schrodinger.com/products/ligprep.
[66] Glide (2020). Schrödinger, Schrödinger Release 2020-3. New York, NY: Schrödinger, LLC. https://www.schrodinger.com/products/glide.
[67] Desmond Molecular Dynamics System (2020) D.E. Shaw Research. New York, NY, 2021. Schrödinger, Maestro-Desmond Interoperability Tools, Schrödinger, New York, NY, 2020. https://www.schrodinger.com/products/desmond.
[68] B. Sureshkumar, Y.S. Mary, K. Resmi, S. Suma, S. Armaković, S.J. Armaković, C. Van Alsenoy, B. Narayana, D. Sobhana, Spectroscopic characterization of hydroxyquinoline derivatives with bromine and iodine atoms and theoretical investigation by DFT calculations, MD simulations and molecular docking studies, J. Mol. Struct. 1167 (2018) 95–106.